Check for updates

Earthquake Engineering & Structural Dynamics

WILEY

RESEARCH ARTICLE OPEN ACCESS

Low-Cost Friction-Based Force-Limiting Connection With Reduced Sensitivity to Machining Tolerances and Accelerated Repairability

Kaixin Chen[1] | Georgios Tsampras[1] | Chung-Che Chou[2] | Huang-Zuo Lin[2] | Chi-Jeng Wu[2] | Alvaro Córdova[2] | Chia-Ming Uang[1] | Shih-Ho Chao[3]

[1]University of California San Diego, San Diego, California, USA | [2]National Taiwan University, Taipei City, Taiwan | [3]University of Texas Arlington, Arlington, Texas, USA

Correspondence: Georgios Tsampras (gtsampras@ucsd.edu)

Received: 9 June 2025 | **Revised:** 10 November 2025 | **Accepted:** 24 December 2025

Keywords: design considerations | experimental testing | force-limiting deformable connections | friction | manufacturing | repairability

ABSTRACT

This paper presents a novel yet practical friction-based structural component design for low-damage earthquake-resistant structures. The proposed connection design is based on a conventional slotted-bolted configuration with the novelty being the use of loose steel washer plates to establish the friction-sliding interface. This design concept offers two key advantages: (1) The connection generates relatively constant sliding forces without the need for small geometric tolerances in the machined parts, and (2) the use of loose steel washer plates to establish the friction interface allows quick inspection and replacement of friction shims if needed. Eliminating the need for small geometric tolerances reduces the manufacturing cost and time. Reducing the inspection and potential repair time enhances the practicality of the connection in real applications and supports the long-term functionality of earthquake-resistant buildings equipped with it. To verify this design concept, a numerical simulation was first conducted to assess the expected kinematics and force-displacement response. A comprehensive experimental characterization program was conducted, which consisted of component-level connection tests and shaking table tests of a full-scale three-story re-centering steel braced frame with sliding slabs, in which the proposed friction-based connection was designed as the force-limiting connection between the steel frame and the sliding slab. It is observed that the proposed connection exhibited a stable force-displacement response and relatively low bolt load loss without enforcing small geometric tolerances when machining the parts of the connection. The replacement of the friction shim was performed after the completion of the shaking table test while the friction-based connection remained installed on the frame specimen, which hence demonstrated the repairability of this connection.

1 | Introduction

1.1 | Friction-Based Structural Components

In earthquake-resistant structures, friction-based structural components are typically designed to be strategically placed along the seismic load path and transfer seismic-induced forces through contact interfaces designed to slide at a predetermined friction force. As a result, the force transferred through friction-based structural components is limited based on the sliding friction force of the friction interface, and energy dissipation is typically associated with sliding. Researchers have developed various designs for friction-based components appropriate for structural engineering applications. For example, in superstructures,

This is an open access article under the terms of the Creative Commons Attribution-NonCommercial-NoDerivs License, which permits use and distribution in any medium, provided the original work is properly cited, the use is non-commercial and no modifications or adaptations are made.

© 2026 The Author(s). *Earthquake Engineering & Structural Dynamics* published by John Wiley & Sons Ltd.

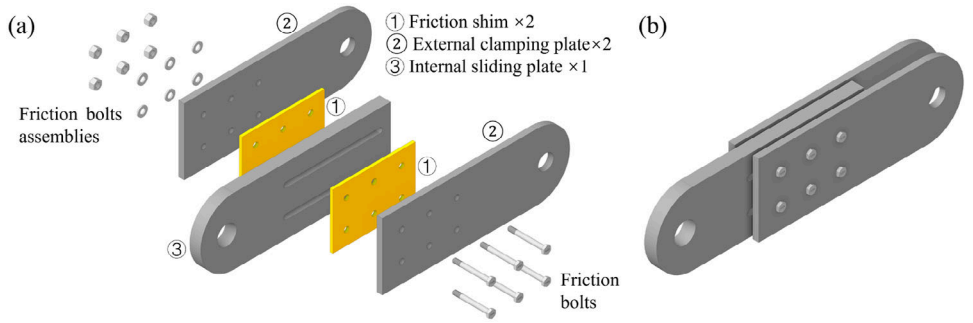


FIGURE 1 | Schematic representation of an example slotted-bolted friction-based structural component: (a) Exploded view and (b) Assembly.

friction-based structural components have been developed as primary structural connections such as force-limiting connections between floor diaphragms and seismic force resisting systems [1–4], as well as supplemental energy dissipation devices [5] such as friction dampers for concrete buildings [6–8], steel buildings [9–12], and timber buildings [13–15]. A more detailed review of these applications is available in the literature [3, 16, 17]. Proprietary friction-based structural components, developed by companies from Canada [18, 19], Denmark [20], Japan [21], and New Zealand [22], have been used in both new building designs and retrofitting projects. Despite the effectiveness demonstrated through research and practice, the underlying mechanics and design considerations of friction-based structural components remain relatively unfamiliar to practicing engineers. Therefore, in the next section, the characteristics and design considerations of friction-based structural components are discussed, with the intention of democratizing the mechanics of friction-based structural components toward the development of non-proprietary designs. The research need of this study is also justified through this discussion.

1.2 | Design Considerations of Friction-Based Structural Components

The short- and long-term force-displacement response of friction-based structural components depends on three considerations: (1) the materials used to establish the friction interfaces, (2) the design and manufacturing of the parts that form the friction-based structural component, and (3) the assembly of the parts into the friction-based structural component. Moreover, in long-term operation, the repairability of the friction-based structural component should be considered. This section discusses these design considerations and focuses specifically on the slotted-bolted configuration, which is one of the most commonly used configurations for friction-based structural components [16]. Figure 1 presents the schematic representation of an example slotted-bolted friction-based structural component. The component shown in Figure 1 was intended to be used as the floor-to-wall force-limiting connection in earthquake-resistant structures [2, 3, 23].

1.2.1 | Friction Interface Materials

Both bimetallic and composite-metallic friction interfaces have been considered for friction-based structural components in earthquake engineering applications. Bimetallic friction interfaces were historically widely characterized and adopted [10, 24], but there have been concerns about their long-term performance because galvanic corrosion and cold welding (i.e., very high adhesion generated at the friction interface due to the formation of solid solutions or intermetallic compounds) developed at the bimetallic friction interface can result in an unstable long-term force-displacement response of the friction-based structural component [25]. Composite-metallic friction interfaces are preferred because they mitigate the potential for the development of galvanic corrosion at the friction interface. If appropriate material pairs are selected, composite-metallic friction interfaces could have controlled wear mechanisms and stable tribological behavior with respect to parameters that can affect the force-displacement response of friction-based structural components, such as the normal load level, the sliding velocity, the velocity profile, and the sliding history [3, 26].

1.2.2 | Force and Displacement Capacities

An advantage of friction-based structural components is that their force and displacement capacities can be adjusted easily according to design targets. In practice, Coulomb's friction equation [27] is typically used to calculate the force generated by a friction-based structural component. From Coulomb's friction equation $f = \mu N$, where f is the friction force, μ is the coefficient of friction, and N is the normal load acting on the friction interface, it can be observed that the force capacity of friction-based structural components can be adjusted by selecting the material pair used for the friction interface (i.e., adjusting μ) or adjusting the normal load acting on the friction interface (i.e., adjusting N). For friction-based components for superstructural applications such as the example shown in Figure 1, the normal load acting on the friction interface is typically applied through the pretension of the structural bolts and could be adjusted by changing the number of the structural bolts or the pretension level of the structural bolts.

The displacement capacity of friction-based structural components can be adjusted by modifying the design of their parts. For example, for the slotted-bolted friction-based structural component in Figure 1, its displacement capacity can be increased simply by increasing the length of slots on the internal sliding plate. This eliminates the strain limitation of materials which is typically a design constraint for metallic-based seismic response modification structural components such as

10969845, 2026, 6, Downloaded from https://onlinelibrary.wiley.com/doi/10.1002/eqe.70121 by University Of California, Wiley Online Library on [07/11/2026]. See the Terms and Conditions (https://onlinelibrary.wiley.com/terms-and-conditions) on Wiley Online Library for rules of use; OA articles are governed by the applicable Creative Commons License

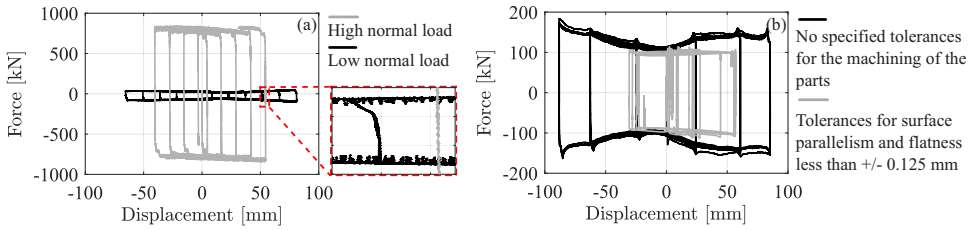


FIGURE 2 | (a) High axial stiffness with two significantly different sliding force levels using the same friction-based structural component. (b) Geometric tolerances used to machine the components of the friction-based structural components may contribute to an uncontrolled variation of the friction force during sliding.

buckling-restrained braces (BRBs) [28] and shape memory alloy (SMA) based components [29].

1.2.3 | Decoupled Elastic Axial Stiffness and Sliding Friction Force

Ideally, friction-based structural components have an elastic-perfectly plastic force-displacement response. The elastic stiffness is effectively independent of the friction force during sliding. Figure 2a shows the force-displacement response of an example slotted-bolted friction-based structural component [3]. The component developed two significantly different force levels while the difference between the elastic axial stiffness was effectively small (for the low normal load and the high normal load cases, the experimentally computed elastic stiffness were 1809 kN/mm and 2245 kN/mm, respectively). The sliding friction force was increased simply by increasing the normal load acting on the friction interface by the bolts. The decoupled elastic axial stiffness and sliding friction force provide structural engineers with enhanced flexibility in practical design.

1.2.4 | Geometric Tolerances

The geometric tolerances associated with the machining of the parts that form the friction-based structural component can contribute to the variation of the sliding friction force beyond the designed sliding friction force. Figure 2b shows the force-displacement response of two friction-based structural components designed to develop a sliding friction force of 100 kN. The friction-based structural component designed with enforced geometric tolerances less than +/-0.125 mm was able to develop a relatively constant friction force during sliding. The low geometric tolerances ensured the flatness and parallelism of the surfaces associated with the friction interfaces and the slots. In contrast, the friction-based structural component designed without specified geometric tolerances developed an uncontrolled displacement-dependent variable friction force during sliding. The reason is the following. When the slots are not parallel within a tolerance, as the displacement increases, the shanks of the bolts that pass through the slots come into contact with the internal surface of the slots. Additional friction force is developed due to the contact force between the bolt shanks and the internal surface of the slot [3]. In addition, the contact force could result in bending of the bolt. Due to bolt bending, the axial strain in the bolt increases, which as a result increases the axial load of the bolt. The increased bolt load increases the friction force during sliding compared to the designed sliding friction force. Note that although the uncontrolled variable friction force could be mitigated through enforced geometric tolerances, extra time and cost might be required during the machining process of the parts.

1.2.5 | Potential Damage Limit States

Friction-based structural components can be essentially damage-free and immediately reusable after earthquakes; however, this requires the parts of the friction-based structural component to be designed against limit states that could potentially lead to mechanical failure. For a friction-based structural component having composite-metallic friction interfaces, the limit states of the metallic parts (which are typically made of structural steel) can be identified through structural analysis and can be designed against using the AISC Steel Construction Manual [30] as a reference. The limit states of friction shims made of composite friction materials should also be considered. Chen et al. [26] discussed the mechanics of the example slotted-bolted friction-based structural component shown in Figure 1 and explained the potential bearing action between the structural bolts and the friction shim. The bearing action could potentially lead to bearing failure and net section tensile failure of the friction shim [3, 26, 31, 32] and should be considered during the design phase.

Note that although designing against limit states associated with the mechanical failure of friction shims is important, friction-based structural components can be designed to be damage tolerant in case that damage to the friction shims occurs. Figure 3 presents the experimental testing result of a slotted-bolted friction-based structural component, in which the friction shim was made of the composite material RF42 [31, 33]. In this test, net section tensile failure of the friction shim was observed, as shown in Figure 3a. Despite the occurrence of net section tensile failure of the friction shim, the friction-based structural component maintained a relatively stable force-displacement response, as presented in Figure 3b. Following the net section tensile failure of the friction shim, no significant reduction in the force resistance was observed. The testing series continued after the net section tensile failure of the friction shim. Figure 3c presents the force-displacement response in the tenth test following the net section tensile failure of the friction shim. It can be observed that the force-displacement response remained overall stable. High-frequency oscillations observed in the force response were mainly attributed to an issue associated with the actuators' hydraulic power supply [31].

10969845, 2026, 6, Downloaded from https://onlinelibrary.wiley.com/doi/10.1002/eqe.70121 by University Of California, Wiley Online Library on [07/11/2026]. See the Terms and Conditions (https://onlinelibrary.wiley.com/terms-and-conditions) on Wiley Online Library for rules of use; OA articles are governed by the applicable Creative Commons License

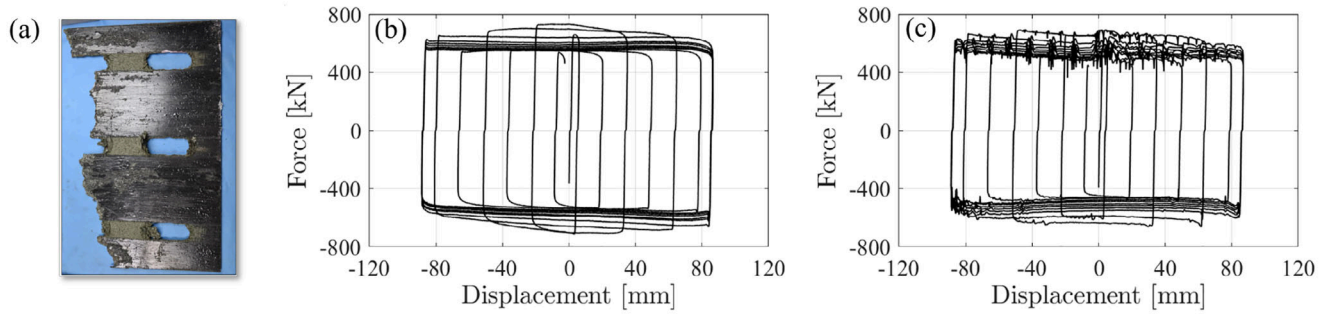


FIGURE 3 | (a) Fractured RF42 friction shim. (b) The force-displacement response of the friction-based component in the test when the fracture of the friction shim first occurred. (c) The force-displacement response of the component in the tenth test following the fracture of the friction shim.

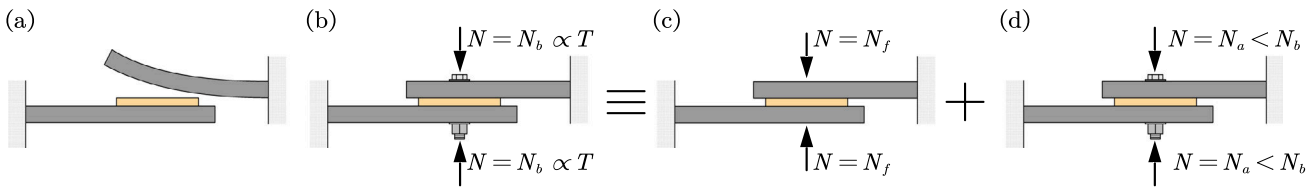


FIGURE 4 | Schematic demonstration of the effect of non-parallel plates on applying the normal load. (a) Initial state of the bolted assembly with a non-flat plate. (b) Final state of the bolted assembly with an applied bolt load $N = N_b$ given an applied tightening torque T ($N_b \propto T$); (b) can be considered as the superposition of (c) and (d). (c) A normal load $N = N_f$ is required to flatten the non-parallel plate. (d) The actual normal load $N = N_a$ acting on the friction interface is effectively smaller than N_b.

1.2.6 | Reliability of Normal Load

As previously discussed, the sliding friction force of a friction-based structural component depends on the normal load acting on the friction interface. For friction-based components for superstructural applications (i.e., excluding the discussion about friction pendulum base isolation systems herein), the normal load is typically applied on the friction interface through the pretension of the structural bolts. This section discusses the reliability of the normal load acting on the friction interface in two stages: at the instant when the normal load is applied and in long-term operation.

In laboratory testing of friction-based structural components, the normal load provided by pretensioned structural bolts can be monitored using through-hole bolt load cells, bolts instrumented with inserted strain gauges, or ultrasonic bolt tension monitors; therefore, the normal load applied can be well monitored and controlled. In practice, the calibrated wrench method [34] can be used for a relatively accurate normal load estimate. Note that when using the calibrated wrench method, the relative parallelism between the parts associated with the friction interface should be considered. Figure 4 presents a schematic demonstration of the effect of non-parallel plates on applying the normal load. Figure 4a represents the initial state of a schematic bolted assembly fixed at both ends and the parts are not perfectly parallel due to a non-flat plate. Figure 4b represents the final state of this bolted assembly. A tightening torque of T is applied to the bolt, resulting in a bolt load of $N = N_b$. In practice, the required tightening torque T for an anticipated bolt pretension N_b is typically calibrated on site [34]. The state of Figure 4b can be considered as the superposition of the states of Figure 4c and d. The total bolt load $N = N_b$ consists of two components: the normal load $N = N_f$ to flatten the non-parallel plate, and the normal load $N = N_a$ effectively acting on the friction interface. It can be observed that, when applying a tightening torque of T to the bolt, if the parts associated with the friction interface are not parallel, the actual normal load effectively acting on the friction interface, i.e., N_a, could be lower than the anticipated normal load, i.e., N_b. The difference between N_a and N_b may be significant in case of thick and short plates with relatively high out-of-plane flexural stiffness.

Figure 5 presents a schematic demonstration of the variation of the bolt load in a bolted assembly in long-term operation. Figure 5a–c presents a simplified model of a bolted assembly. The bolt is idealized as a spring, and the clamped parts are idealized as a spring and a dashpot connected in series [35]. Figure 5a represents the initial state of the bolted assembly when the bolt is not pretensioned. From Figure 5a to Figure 5b, the bolt is pretensioned to a bolt load of P_i. The pretensioning of the bolt results in an elongation of δ_b^i in the bolt and a through-thickness compressive deformation of δ_p^i in the clamped parts. In this state, the kinematic compatibility between the bolt and the clamped parts in the through-thickness direction can be assumed to be satisfied. Figure 5c represents the state of the bolted assembly in long-term operation, where a through-thickness deformation of ΔD_c is further induced, which results in the shortening of the bolt and an increased through-thickness compressive deformation of the clamped parts. Figure 5d presents the force-deformation diagram [35] of the bolted assembly. In Figure 5d, K_b represents the axial stiffness of the bolt-washer assembly. K_p^i and K_p^o represent the through-thickness compressive stiffness of the clamped parts before and after the long-term through-thickness deformation ΔD_c happens. It can be observed that with the long-term through-thickness deformation ΔD_c, the bolt load drops

10969845, 2026, 6, Downloaded from https://onlinelibrary.wiley.com/doi/10.1002/eqe.70121 by University Of California, Wiley Online Library on [07/11/2026]. See the Terms and Conditions (https://onlinelibrary.wiley.com/terms-and-conditions) on Wiley Online Library for rules of use; OA articles are governed by the applicable Creative Commons License

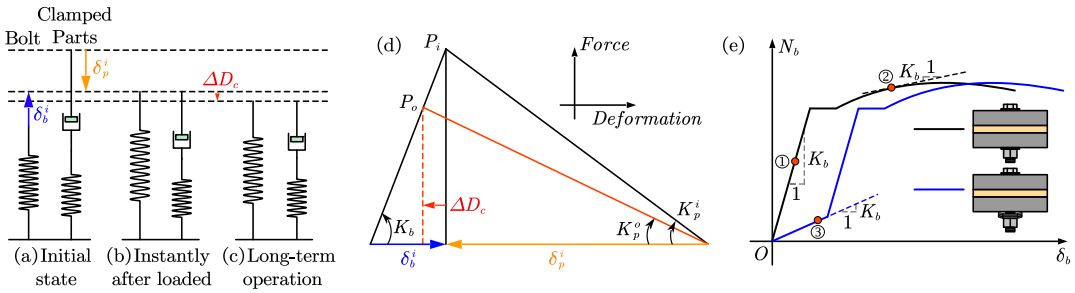


FIGURE 5 | Schematic demonstration of long-term bolt relaxation in a bolted assembly. (a) The initial state of a simplified model of a bolted assembly. (b) The state of the bolted assembly instantly after the pretensioning of the bolt. (c) The state of the bolted assembly in long-term operation (d) Schematic force-deformation diagram of the bolted assembly. (e) Schematic force (N_b)-deformation(δ_b) response of the the bolt-washer assembly.

from P_i to P_o. The bolt load loss can be written as $\Delta P = P_i - P_o = K_b \Delta D_c$. In friction-based structural components, this mechanism is related to the loss of the normal load acting on the friction interface in long-term operation.

The long-term through-thickness deformation ΔD_c primarily depends on the through-thickness creep behavior of the clamped parts. ΔD_c can be assessed and predicted but cannot be fully avoided [36–39]. From the expression of ΔP and considering a same amount of ΔD_c, it can be observed that one way to mitigate the bolt load loss (i.e., to reduce ΔP) due to ΔD_c is to increase the axial flexibility (i.e., to reduce K_b) of the bolt-washer assembly. Bolted assemblies with Belleville washers or disc springs (as represented by marker ③ in Figure 5e) have been used in friction-based structural components to mitigate the bolt load loss due to ΔD_c in past research [40–44]. One shortcoming of using Belleville washers is that since the flat load of Belleville washers is relatively low, when having an application where a relatively large sliding friction force capacity is required, the designer will have to increase the number of bolts or to stack the Belleville washers to meet the normal load demand. This could increase the cost of the friction-based structural component and sometimes make the design impractical. Another alternative is to use bolt-washer assemblies with flat washers and to pretension the bolt to a bolt load larger than its yield strength [3]. From Figure 5e, it can be observed that by pretensioning the bolt to a bolt load above its yield strength (i.e., from marker ① to ②), the stiffness of the bolt-washer assembly K_b can be effectively reduced. This method is considered more suitable for applications where a relatively large normal load demand is to be met.

1.2.7 | Inspection and Repairing in Long-Term Operation

As discussed in Section 1.2.5, when properly designed, friction-based structural components can be essentially damage-free and immediately reusable after earthquakes. However, in long-term operation particularly after seismic events, the friction shims of the friction-based structural component might require inspection and replacement if mechanical failure occurs or if excessive surface wear is observed. For the slotted-bolted friction-based structural component in Figure 1, the inspection and replacement of the friction shims require the external clamping plate of the component to be removed, which can be practically challenging if the friction-based component has been installed in the structure. Therefore, it is beneficial to have a configuration of the friction-based structural component that allows a quicker inspection and repairing process. A quick inspection and repairing of the friction-based structural component potentially enhances the practicality of the connection in real applications and supports the long-term functionality of earthquake-resistant buildings equipped with it.

1.3 | Summary

As discussed in Section 1.2, for the slotted-bolted friction-based structural component shown in Figure 1 (termed the conventional design herein), it has the following advantage: easily adjusted force and displacement capacities, decoupled elastic axial stiffness and sliding friction force, which provide structural engineers with enhanced flexibility in practical design, and being damage tolerant. However, to ensure a stable and predictable force-displacement response, a couple of design considerations should be taken into account. The material pair to establish the friction interface should be carefully selected. Damage limit states of the parts should be identified and designed against. Reliability of the normal load acting on the friction interface should be considered both at the instant when the normal load is applied and in long-term operation. Geometric tolerances associated with the machining of the parts should be specified, although this requirement may introduce additional time and cost to the manufacturing process. The inspection and replacement of friction shims should be considered in long-term operation, but in practice this could be challenging for the conventional design if the component has been installed in the structure, as it requires removal of the external clamping plate.

2 | Scope of Study

Based on the design considerations and challenges presented in Section 1, the objective of this study is to present the development and experimental characterization of a novel yet practical design concept of a slotted-bolted friction-based structural component that is low-cost, less sensitive to machining tolerances, and easily repairable. The design concept is presented, and the experimental results are discussed. The experimental testing program consisted of two test phases. The first test phase was component-level connection tests. The second test phase was a full-scale shaking table test where the proposed friction-based component was designed as the force-limiting connection

10969845, 2026, 6, Downloaded from https://onlinelibrary.wiley.com/doi/10.1002/eqe.70121 by University Of California, Wiley Online Library on [07/11/2026]. See the Terms and Conditions (https://onlinelibrary.wiley.com/terms-and-conditions) on Wiley Online Library for rules of use; OA articles are governed by the applicable Creative Commons License

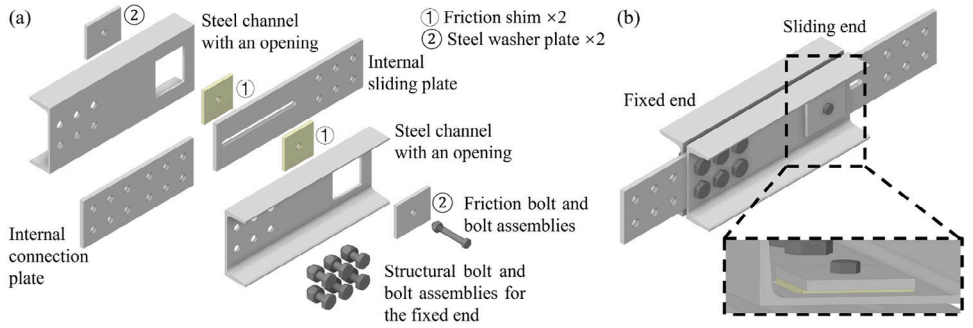


FIGURE 6 | Schematic representation of the proposed friction-based force-limiting connection: (a) Exploded view and (b) Assembly.

between a re-centering steel braced frame and sliding slabs. Throughout the experimental testing program, the performance of the friction-based force-limiting connection designed using this concept was assessed. The repairability of the connection was specifically examined during the shaking table test and is also discussed in this paper. To provide insights into the practical implementation of buildings equipped with friction-based connections designed with this concept, this paper also assesses and reports the reference time required for manufacturing, assembling, installing, and repairing the proposed connection. Note that the characterization of composite-metallic friction interfaces and the long-term bolt load loss of friction-based structural components have been investigated in separate studies [3, 26] and are beyond the scope of this paper.

3 | Design Concept

3.1 | Connection Configuration

Figure 6 presents the schematic representation of the exploded view and the assembly of the proposed friction-based force-limiting connection, which has a slotted-bolted configuration. Two ends of this connection are termed the fixed end and the sliding end, respectively. On the fixed end, two steel channels and one internal connection plate are connected using six structural bolts and bolt assemblies including nuts and flat washers for structural applications. The structural bolts are expected to be ASTM F3125 Gr.A325 medium-strength steel heavy hex head bolts which are commonly used for structural applications in the United States. For each steel channel, a rectangular-shaped opening is created in the channel, in which the friction shim is hosted. Sliding occurs on the end where friction shims are hosted, termed the sliding end. On the sliding end, the friction shims are clamped against the slotted internal sliding plate by initially loose steel washer plates (termed steel washer plates in Figure 6 and herein) and one structural bolt (termed the friction bolt herein) and its bolt assemblies including one nut and one flat washer for structural applications. The friction bolt is also expected to be an ASTM F3125 Gr.A325 structural bolt. The friction interface is formed between the friction shims and the internal sliding plate. The friction bolt and bolt assemblies apply the normal load acting on the friction interface, and loose steel washer plates are clamped to distribute the applied normal load onto friction shims. The friction shims are expected to be made of fiber-reinforced non-metallic composite friction materials [3, 26]. The internal connection plate, the internal sliding plate, and the steel washer plates are expected to be made of commercially available structural steel such as A36 or A572 Gr.50 steel used in the United States. The steel channels are commercially available hot-rolled steel channels, also made of structural steel.

Figure 7 presents the load path of the friction-based connection, considering the connection under tension as a demonstration. Assuming that the normal load acting on the friction interface is N and the coefficient of friction of the friction interface is μ, based on Coulomb's friction equation, the connection generates a friction force $f = 2\mu N$ when sliding, as shown in Figure 7a. For this connection, the parts on the fixed end, i.e., the internal connection plate, two steel channels, and six structural bolts and their assemblies, are expected to remain static relative to each other. On the sliding end, when the steel channels start moving relative to the internal sliding plate, the steel channels make contact with the edge of the friction shims and push the friction shims to move relative to the internal sliding plate and to activate the sliding friction mechanism, as shown in Figure 7b. Therefore, when sliding occurs, the friction shim is under the normal load from bolt pretension, the edge bearing force from the steel channel, and the sliding friction force from the friction interface, as shown in Figure 7c. The bearing force f_{bearing} is distributed on the cross section of the friction shim over an area of A_{contact} and A_{contact} is equal to the product of the thickness of the web of the steel channel and the height of the friction shim. During sliding, the steel channels are not expected to make contact with steel washer plates (as the friction shim thickness is greater than the web thickness of the steel channel) and the internal sliding plate.

In practical design, the required sliding force of this connection should be determined through system-level structural analysis or by following specific design methods, such as those outlined in Section 3 of Chou et al. [45] or in Tsampras and Sause [46]. A detailed discussion of how to determine the required sliding force is beyond the scope of this paper. At the component level, damage limit states of the connection parts should be considered, and the parts should be sized based on the required sliding force. On the fixed end, the connection between the internal connection plate and the steel channels should be designed as a slip-critical connection in accordance with Section J3 of AISC 360-22 [47], and the strength requirements of both the structural bolts and plates should be satisfied. On the sliding end, given the required sliding force (f) and the selected material pair for the friction interface (μ), the required bolt pretension acting on the friction interface (N) can be calculated using Coulomb's friction

10969845, 2026, 6, Downloaded from https://onlinelibrary.wiley.com/doi/10.1002/eqe.70121 by University Of California, Wiley Online Library on [07/11/2026]. See the Terms and Conditions (https://onlinelibrary.wiley.com/terms-and-conditions) on Wiley Online Library for rules of use; OA articles are governed by the applicable Creative Commons License

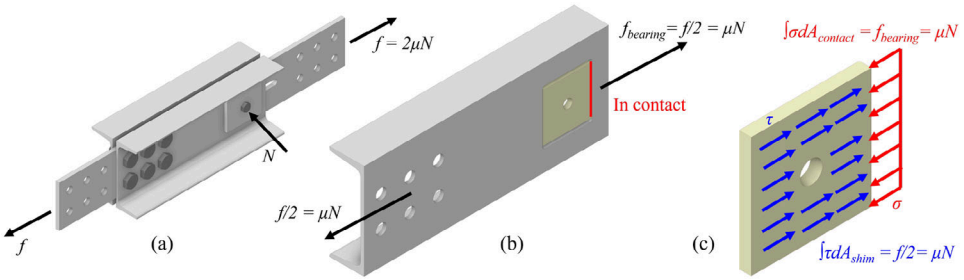


FIGURE 7 | Load path of the friction-based connection: (a) The connection generates a tensile force of $f = 2\mu N$. (b) Schematic free body diagram of the steel channel when in contact with the friction shim in the opening. (c) Schematic free body diagram of the friction shim (The normal load acting on the friction shim is not shown in the figure).

equation ($N = f/\mu$). The resulting nominal normal pressure acting on the friction shim should be checked. Past research [3, 26] has suggested that for friction shims made of fiber-reinforced composite materials, 13.5 MPa is a reasonable reference upper limit for the nominal normal pressure. The friction shim should have sufficient bearing strength to resist the bearing action from contact with the steel channel, as well as adequate shear strength to resist the in-plane shear stress induced by the friction force. The steel channels and the internal sliding plate should have sufficient design tensile and compressive strengths to resist connection forces, and the design tensile and compressive strengths can be computed following Sections D and E of AISC 360-22 [47], respectively. Note that when the friction shim is in contact with the steel channel and when the connection is in tension, as shown in Figure 7b, stress concentration could be developed locally at the outer edge of the steel channel in the direction of loading close to the opening, and result in critical regions of high stress. This effect should be taken into account when detailing the steel channel.

The design concept shown in Figure 6 has several advantages. First, the parts of this connection, i.e., the steel plates and hot-rolled steel channels, are commercially available and relatively low-cost. Second, the sliding friction mechanism is activated through the bearing action between the steel channel and the edge of the friction shim. In contrast, for the conventional design of slotted-bolted friction-based structural components shown in Figure 1, the bearing action typically occurs between the friction bolt and the friction shim. The bearing action between the friction bolt and the friction shim leads to the variation of the axial strain in the bolt and potential damage to the friction shims (see Figure 3a). The activation of sliding through bearing between the edge of the friction shim and the steel channel, as shown in Figure 7b and c, reduces the chance of friction shim damage and reduces the variation of the axial strain in the friction bolt. In addition, the initially loose steel washer plates are clamped to apply confining pressure on the friction shim that helps prevent the development of damage due to bearing. Third, the design with loose steel washer plates mitigates the effect of non-parallel plates on applying the normal load as demonstrated in Figure 4. This allows for a more accurate normal load estimate when applying the normal load using the calibrated wrench method in practice. Fourth, the design with loose steel washer plates increases the flexibility between the internal sliding plate and the assembly with friction shims, steel washer plates, and the friction bolt and its assemblies. The increased flexibility mitigated the effect of the contact between the internal surface of the slot and the friction bolt on the response of the connection; therefore, the parts of the connection, i.e., the internal sliding plate, the steel channels, and the steel washer plates, do not need to be machined following a low geometric tolerance with respect to their flatness and parallelism. Compared to the example conventional design in Figure 1, this design concept reduces the time and cost of machining the parts. Lastly, compared to the example conventional design of slotted-bolted friction-based components in Figure 1 of which the repairing and inspection requires to remove the external clamping plate, the design with loose steel washer plates allows for quicker inspection and replacement of the friction shims after an earthquake if needed.

3.2 | Preliminary Numerical Assessment of the Design Concept

As an intermediate step in the development of the proposed friction-based connection, a numerical simulation was performed in the ANSYS Mechanical finite element software [48], with the objective of preliminarily assessing both the expected kinematics of the connection and its anticipated force–displacement response. In the numerical simulation, the internal connection plate, the steel channels, the friction shims, and the steel washer plates were explicitly simulated using eight-node solid finite elements. The bolts for the fixed end, the friction bolt, and the bolt assemblies were not explicitly simulated. The pretension of the friction bolt was 50 kN, being simulated as a constant force boundary condition distributed to the nodes on the surface of the elements in the steel washer plates. The contact interfaces between the modeled parts were explicitly simulated using pair-based contact definition. A contact pair was defined between each surface of the friction shims and the adjacent surface of the internal sliding plate; for those contact pairs, a Coulomb-type frictional behavior was defined with a constant coefficient of friction equal to 0.4. The sliding force of the connection was computed using the modified version of Coulomb's friction equation $f = n_b n_s \mu N$, where n_b was the number of the friction bolt and was equal to 1; n_s was the number of the friction interface that contributes to the sliding friction force and was equal to 2; μ was the expected coefficient of friction, 0.4; and N was the normal load acting on the friction interface provided by one bolt, which was 50 kN. The resulting sliding force of the connection f was equal to 40 kN.

10969845, 2026, 6, Downloaded from https://onlinelibrary.wiley.com/doi/10.1002/eqe.70121 by University Of California, Wiley Online Library on [07/11/2026]. See the Terms and Conditions (https://onlinelibrary.wiley.com/terms-and-conditions) on Wiley Online Library for rules of use; OA articles are governed by the applicable Creative Commons License

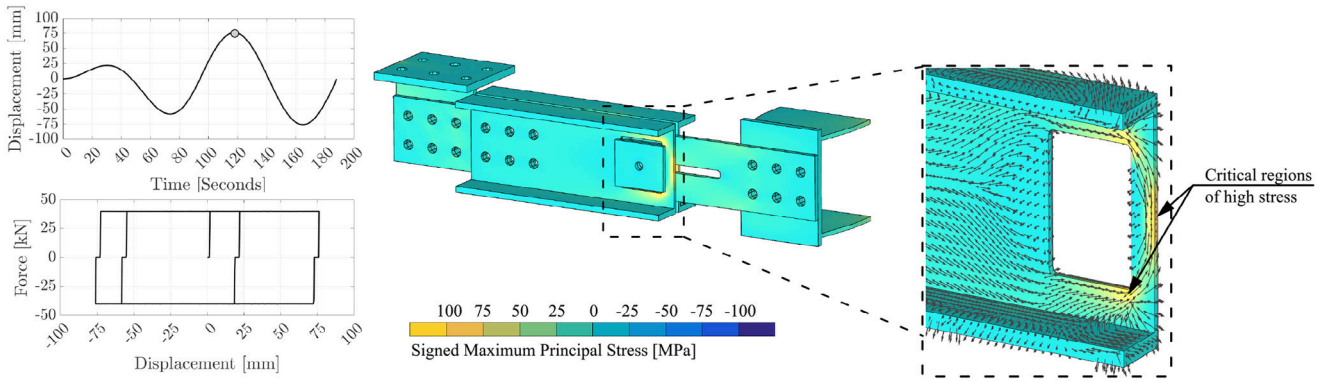


FIGURE 8 | Numerical simulation of the proposed friction-based connection.

In the numerical simulation, static structural analysis was performed. Figure 8 presents the imposed displacement time history of the analysis and the resulting force-displacement response of the connection. In the force-displacement response plot, positive force indicates tension in the connection. The force-displacement response overall resembled a Coulomb-type frictional behavior. In the force-displacement response, zero-force pinching displacement was observed due to the gap between the friction shim and the steel channel. In practice, the zero-force pinching displacement in the force-displacement response can be reduced by enforcing a tighter tolerance when machining the opening on the steel channel. The maximum principal stresses in the connection when the imposed displacement was equal to +75 mm and when the connection was under tension is also presented in Figure 8. From the maximum principal stresses results, critical regions of high stress can be identified and they are at the outer edge of the steel channel in the direction of loading close to the opening and at the inner corner of the opening. The magnitude of the maximum principal stresses at these regions can be reduced by increasing the radius of the inner corner of the opening and by increasing the width of material between the inner and outer edge of the steel channel.

4 | Experimental Program

4.1 | Summary of Testing Phases

Table 1 presents the testing phases of this experimental study. Test Phase 1 included component-level connection tests conducted at the University of California San Diego and consisted of three test groups. The main objective of Test Phase 1 was to experimentally validate the proposed friction-based connection design and to support Test Phase 2. Test Phase 2 was conducted at the National Center for Research on Earthquake Engineering (NCREE) in Taiwan, which was the shaking table tests of a three-story, re-centering steel braced frame with sliding slabs, where the proposed friction-based connection was designed to work as the force-limiting connection between the steel frame and sliding slabs. Test Phase 2 also included pre-shaking table tests or post-shaking table tests of the connection. The target connection sliding force was 40 kN in all tests. The target connection sliding force was estimated based on the force required to be transferred between the steel frame and sliding slabs. Per Section 3.1, if needed, a higher connection sliding force can be achieved by increasing the normal load acting on the friction interface, and the parts of the connection can be sized and detailed accordingly. For example, Chen et al. [26] detailed a connection following the same design concept for the characterization of the tribological properties of phenolic-resin-based composite materials that required a connection sliding force of more than 200 kN.

4.2 | Test Phase 1: Component-Level Connection Test

4.2.1 | Manufacturing of the Connection Specimen

This section presents the manufacturing process of the parts of the connection specimen used in Test Phase 1. The connection specimens used in Test Phase 2 were manufactured following a similar process. For the connection specimen used in Test Phase 1, the steel channels, the internal sliding plate, the internal connection plate, and the steel washer plates, were all made of A36 low-carbon structural steel. A Computer Numerical Controlled (CNC) subtractive manufacturing approach was used for machining the steel parts. The toolpath programming was completed using Autodesk Fusion 360 [49] and the machining of the steel parts was completed in the machining shop of the University of California San Diego using a HAAS VF4 vertical machining center [50]. The steel channels for the connection specimen were commercially available C10×15.3 hot-rolled steel channels, of which the cross-sectional dimensions followed the AISC Steel Construction Manual [30]. The length of each channel was 635 mm (25 inch). The machining process of the steel channel involved creating the rectangular-shaped opening and the bolt holes on the channel. The rectangular-shaped opening had a dimension of 130 mm × 143 mm to host the friction shim of which the dimension was 127 mm × 127 mm × 12.7 mm (5 inch × 5 inch × 0.5 inch). A 2D pocket toolpath was selected and programmed to complete the machining task. The internal sliding plate had a dimension of 508 mm × 203.2 mm × 12.7 mm (20 inch × 8 inch × 0.5 inch) and was cut from a raw material stock plate having a dimension of 609.6 mm × 254 mm × 12.7 mm (24 inch × 10 inch × 0.5 inch). The machining process of the internal sliding plate involved two steps: the first step was to create the slot on the plate using the 2D pocket toolpath and the second step was to use the 2D contour toolpath to cut the internal sliding plate off the raw material stock plate. It is worth noting that for the internal

10969845, 2026, 6, Downloaded from https://onlinelibrary.wiley.com/doi/10.1002/eqe.70121 by University Of California, Wiley Online Library on [07/11/2026]. See the Terms and Conditions (https://onlinelibrary.wiley.com/terms-and-conditions) on Wiley Online Library for rules of use; OA articles are governed by the applicable Creative Commons License

TABLE 1 | Test phases of the proposed friction-based connection.

Test phase	Test group	No. of tests	Objectives
1 Component-level connection test	1	63	Preliminary experimental evaluation of the feasibility of the proposed friction-based connection design
	2	32	Investigation of the friction bolt load variation and the response of the friction-based connection under earthquake-type input excitation
	3	7	Verification of the proposed break-in process for the friction-based connection
2 Shaking table test	1	6	Pre-shaking-table-test break-in process of the friction-based connection
	2	8	Shaking table test of a steel frame equipped with proposed friction-based connections
	3	6	Post-shaking-table-test investigation of the response of the friction-based connection
	4	2	Connection test 10 months after the shaking table test to assess the aging effect

TABLE 2 | Information about the machining of the parts of the connection specimen used in Test Phase 1.

Manufacturing machine	Part	Number of parts machined	Reference machining time [min]
HAAS VF-4	Steel channel	2	89.2
	Internal sliding plate	1	23.4
	Internal connection plate	1	28.8
	Steel washer plate	2	3.7
Onefinity CNC milling system	Friction shim	16	281.8

sliding plate, geometric tolerances with respect to its flatness and parallelism were not enforced; the surfaces of the internal sliding plate associated with the friction interface were not face milled during the machining process. The internal connection plate had a dimension of 355.6 mm × 203.2 mm × 12.7 mm (14 inch × 8 inch × 0.5 inch) and was also cut from a raw material stock plate having a dimension of 609.6 mm × 254 mm × 12.7 mm (24 inch × 10 inch × 0.5 inch). The machining of the internal connection plate involved creating bolt holes on the plate using the 2D pocket toolpath and cutting the plate off the raw material stock plate using the 2D contour toolpath. The steel washer plate had a dimension of 152.4 mm × 152.4 mm × 12.7 mm (6 inch × 6 inch × 0.5 inch) and the raw material stock plate had the same dimension. The machining process of the steel washer plate just required creating the bolt hole on the plate using the 2D pocket toolpath. Table 2 summarizes the reference machining time of the parts. The reference machining time considers only the time spent on machining operations but does not take the time spent on other operations (e.g., workholding setup and probing) into account. In the machining of all the steel parts, a TiAlN-coated 4-flute carbide end mill with a diameter of 12.7 mm (0.5 inch) was used for all the machining operations. For 2D pocket toolpaths, the cutting parameters used were: spindle speed = 1,000 RPM, resulting in a surface speed of 0.665 m/s (130.9 ft/min); cutting feed rate = 1,016 mm/min (40 inch/min), resulting in a chip load of 0.254 mm per tooth (0.01 inch per tooth); the cutting depth was 1.27 mm (0.05 inch) per pass. For 2D contour toolpaths, the cutting parameters used were: spindle speed = 4,393 RPM, resulting in a surface speed of 2.921 m/s (575 ft/min); cutting feed rate = 1,517.4 mm/min (59.74 inch/min), resulting in a chip load of 0.0864 mm per tooth (0.0034 inch per tooth); the cutting depth was 2.54 mm (0.1 inch) per pass.

For the friction-based connection tested in this study, the friction interface was formed by low-carbon structural steel (A36 steel) in contact with the composite friction material Gatke 398 [51] manufactured by ScanPac Mfg., Inc., which consisted of phenolic resin matrix, E-glass fiber cloth reinforcement, lubricants including graphite, Teflon, and molybdenum disulfide (MoS_2), and fillers. A systematic characterization of the mechanical and tribological properties of six composite friction materials showed that the Gatke 398 to low-carbon structural steel friction interface exhibits stable frictional behavior [26]. The friction shim had a dimension of 127 mm × 127 mm × 12.7 mm (5 inch × 5 inch × 0.5 inch). The thickness of the friction shim should be enough to prevent the steel channel from getting in contact with the steel washer

10969845, 2026, 6, Downloaded from https://onlinelibrary.wiley.com/doi/10.1002/eqe.70121 by University Of California, Wiley Online Library on [07/11/2026]. See the Terms and Conditions (https://onlinelibrary.wiley.com/terms-and-conditions) on Wiley Online Library for rules of use; OA articles are governed by the applicable Creative Commons License

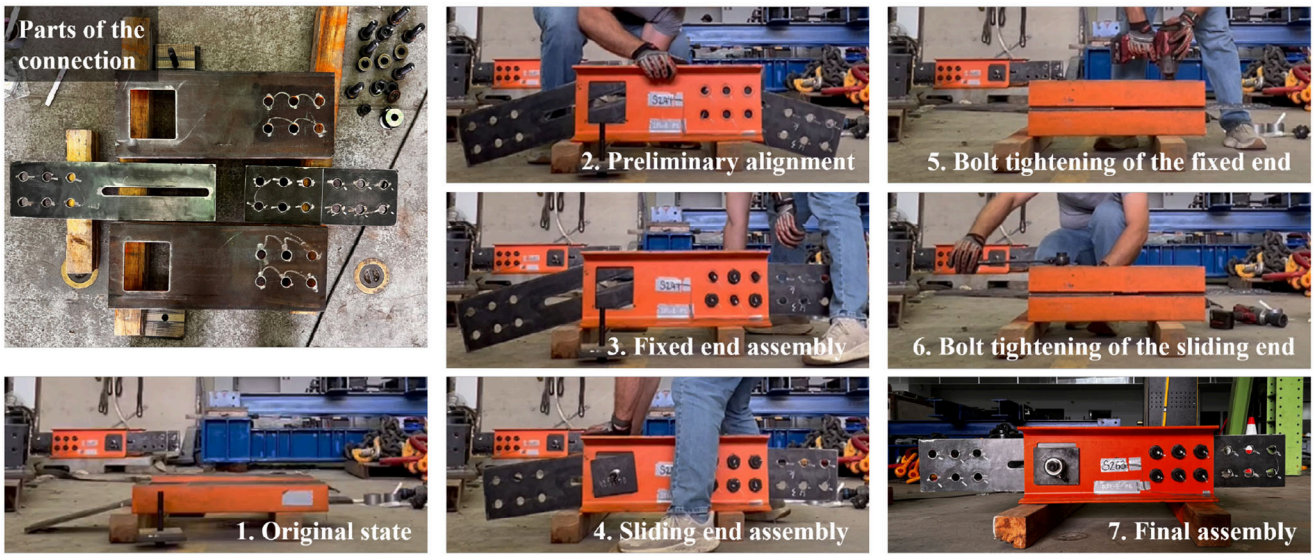


FIGURE 9 | Connection assembly demonstration.

plate. A dry CNC subtractive manufacturing approach was used to machine the friction shims. A three-axis Onefinity [52] CNC milling system with a diamond-coated end mill was used for the machining process. Details regarding the Gatke 398 material properties, specimen preparation, and cutting parameters have been provided in Chen et al. [26].

4.2.2 | Assembly of the Connection

Figure 9 demonstrates the assembly process of the proposed friction-based connection. The parts of the connection were initially roughly positioned for preliminary alignment. The structural bolts and bolt assemblies were then inserted on the fixed end and loosely tightened to position the internal connection plate with respect to the two steel channels. On the sliding end, the internal sliding plate was elevated to its designated position. The friction shims were then placed in the openings on the steel channels against the internal sliding plate and the steel washer plates were also held in position. The friction bolt and its bolt assemblies were then put in and the friction bolt was loosely tightened to assemble the sliding end. Once all parts were properly positioned, the bolts for the fixed end were tightened at their minimum pretension level to ensure that there was no relative movement between the parts on the fixed end. The friction bolt was then tightened to the designed target normal load level based on the specific required sliding force of the connection. For the connection used in this study, as previously mentioned, the target connection sliding force was 40 kN. For the Gatke 398 to low-carbon structural steel friction interface, a reference coefficient of friction μ was 0.4 [3, 26, 51]. The target normal load was calculated to be 50 kN (approximately 30% of the minimum pretension of the friction bolt in this case) and the normal load could be applied using a manual torque wrench to pretension the friction bolt, as shown in Figure 9. For higher target normal loads, an electric or hydraulic torque wrench might be required for the pretensioning process. The entire assembly process was completed by a single worker and took approximately three minutes.

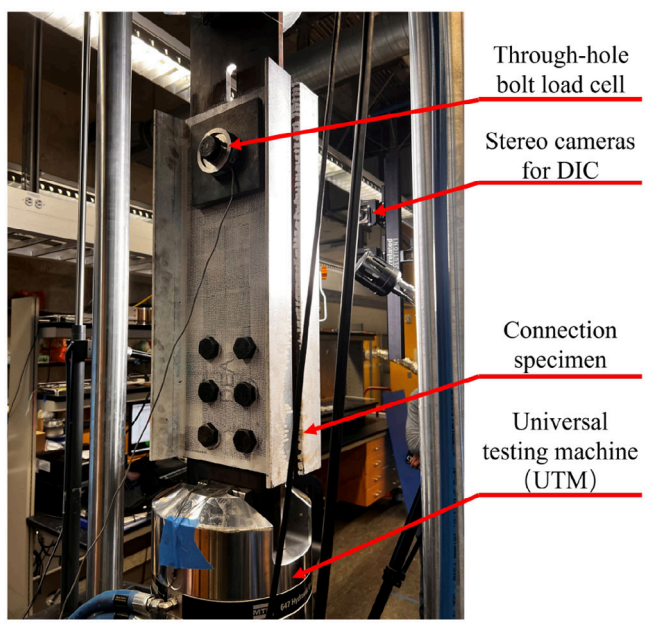


FIGURE 10 | Representative connection test setup.

4.2.3 | Connection Test Setup and Instrumentation

Figure 10 presents the connection test setup of Test Phase 1. The connection tests conducted in Test Phase 2 adopted a similar test setup. The connection tests were conducted using a universal testing machine (UTM). The instrumentation of the connection test was adapted to the objective of each test group. In all connection tests, the connection displacement and the connection force were recorded using the UTM controller. The connection deformation and sliding motion were effectively equal to the UTM actuator displacement. The connection force was effectively equal to the UTM actuator load. In addition to the force and displacement data, imaging data was collected in Test Group 1. Digital Image Correlation (DIC) method was used to compute the full-field strain responses using the imaging data.

10969845, 2026, 6, Downloaded from https://onlinelibrary.wiley.com/doi/10.1002/eqe.70121 by University Of California, Wiley Online Library on [07/11/2026]. See the Terms and Conditions (https://onlinelibrary.wiley.com/terms-and-conditions) on Wiley Online Library for rules of use; OA articles are governed by the applicable Creative Commons License

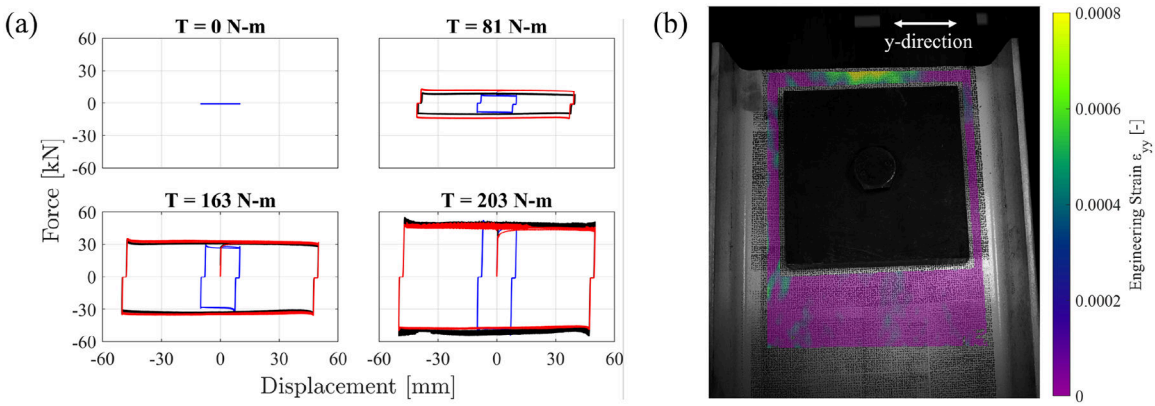


FIGURE 11 | (a) Selected force-displacement responses of the connection in Test Phase 1 Test Group 1. (b) Selected DIC analysis results of Test Group 1.

The strain field computed using the Test Group 1 imaging data was compared with the strain field computed using the numerical model. Imaging data was not collected in follow-up connection tests. In Test Groups except for Test Group 1, a through-hole bolt load cell was used to monitor the bolt load of the friction bolt throughout the test.

4.2.4 | Results

Test Phase 1 Test Group 1 served as a preliminary experimental evaluation of the feasibility of the proposed friction-based connection design. Sixty-three displacement-controlled cyclic tests were completed and ramped sinusoidal displacement time histories were used as the input excitation. Two loading frequencies (0.03 Hz and 0.20 Hz), six peak displacements (10 mm, 20 mm, 30 mm, 40 mm, 50 mm, and 58 mm), and seven levels of the applied torque T (bolt was not preloaded (0 N-m), bolt was hand tightened, 81 N-m, 163 N-m, 183 N-m, 203 N-m, and 217 N-m) on the friction bolt were considered. Figure 11a presents selected connection force-displacement response results of Test Phase 1 Test Group 1. In Figure 11a, each subplot corresponds to one level of the applied torque on the friction bolt (from top left to bottom right: bolt was not preloaded (0 N-m), 81 N-m, 163 N-m, and 203 N-m). Blue lines represent force-displacement responses of the connection in tests having a loading frequency of 0.03 Hz and a peak displacement of 10 mm; black lines represent force-displacement responses of the connection in tests having a loading frequency of 0.03 Hz and a peak displacement of either 40 mm or 50 mm; red lines represent force-displacement responses of the connection in tests having a loading frequency of 0.20 Hz and a peak displacement of either 40 mm or 50 mm. The result of the $T = 0$ N-m case shows that when the friction bolt was not preloaded, the friction force between the parts of this connection could be considered negligible. The results of the rest of the tests show that regardless of the loading frequency, the peak displacement, and the value of the applied torque on the friction bolt, the proposed friction-based connection exhibited stable force-displacement responses (i.e., the connection generated a relatively constant sliding friction force without exhibiting the uncontrolled displacement-dependent variable friction force shown in Figure 2b). The force-displacement response of the proposed connection was close to a rectangle; therefore, a Coulomb-type frictional behavior idealization could be used for this connection in practical design. Importantly, with this novel design concept, the force-displacement response of the connection did not exhibit an uncontrolled variable friction force as shown in Figure 2b even when the parts were not machined following a low geometric tolerance with respect to their flatness and parallelism.

The commercial software Vic-3D [53] was used for the DIC analysis in Test Phase 1 Test Group 1. Figure 11b shows a selected representative DIC analysis result. The frame selected was from Test 34 of Test Group 1 when the applied torque T was equal to 163 N-m and represented a moment when the connection was in tension. The contour map of the engineering strain ε_{yy} is shown in Figure 11b. The DIC analysis results provided experimental validation of the numerical simulation (Figure 8), confirming that high stress concentrations developed near the outer edge of the steel channel adjacent to the opening in the direction of loading without exceeding the yield strain limit.

Gatke 398 friction shims conditions were inspected throughout the testing. Figure 12a and b present the representative surface and edge appearance of Gatke 398 friction shims before and after the test, respectively. The Gatke 398 friction shims were observed to be damage free. No mechanical failure or damage was observed on the surface of the friction shim which formed the friction interface, or the edge of the friction shim where the bearing action between the steel channel and the friction shim was established. Black wear marks were observed on the surface of the friction shim that formed the friction interface, which resulted from the thermo-oxidative degradation process of the phenolic resin constituent [26, 54].

Following Test Group 1, Test Group 2 was conducted to further investigate the connection response, taking earthquake-type input excitation and the variation of the friction bolt load into consideration. Table 3 presents the loading protocol of Test Group 2. In Test Group 2, Tests 1, 2, 3, 13, 14, and 15 had expected seismic-induced responses of a friction-based structural connection as the imposed displacement time histories of the input excitation. The imposed displacement time histories for these tests were responses of a friction-based structural connection from numerical earthquake simulations of the steel frame in Test Phase 2

10969845, 2026, 6, Downloaded from https://onlinelibrary.wiley.com/doi/10.1002/eqe.70121 by University Of California, Wiley Online Library on [07/11/2026]. See the Terms and Conditions (https://onlinelibrary.wiley.com/terms-and-conditions) on Wiley Online Library for rules of use; OA articles are governed by the applicable Creative Commons License

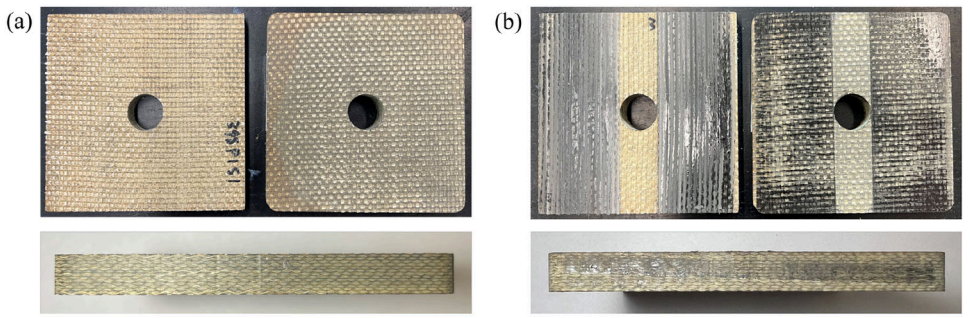


FIGURE 12 | Representative surface and edge appearance of Gatke 398 friction shims (a) Before a test and (b) After a test.

TABLE 3 | Loading protocol of Test Phase 1 Test Group 2.

Test ID	Input type	Peak displ. [mm]	Peak vel. [mm/sec]	Loading freq. [Hz]	Descriptions
0	Ramped Sine	50	7.6	0.0243	Bolt was not preloaded, as a pre-test set-up check
1	EQ-DBE	22	~28	—	Assess the connection response at DBE level earthquake
2	EQ-MCE	31	~35	—	Assess the connection response at MCE level earthquake
3	EQ-1.5MCE	52	~36	—	Assess the connection response at 1.5 × MCE level earthquake
4~12	Ramped Sine	Various	Various	Various	Assess the connection response under ramped sinusoidal motions with various peak displacements, peak sliding velocities, and loading frequencies
13	EQ-1.5MCE	52	~36	—	Assess repeatability of the connection response at 1.5 × MCE level earthquake, compared to Test 3
14	EQ-DBE	22	~28	—	Assess repeatability of the connection response at DBE level earthquake, compared to Test 1
15	EQ-MCE	31	~35	—	Assess repeatability of the connection response at MCE level earthquake, compared to Test 2

[55] considering three levels of ground motion intensities (Design Basis Earthquake (DBE), Maximum Considered Earthquake (MCE) and 1.5 times Maximum Considered Earthquake (1.5 × MCE)). The sliding velocity imposed by the displacement histories was scaled down to be limited below the testing machine's capacity by elongating the duration of the displacement histories. The velocity-dependent frictional behavior of the Gatke 398 to low-carbon structural steel friction interface has been discussed in Chen et al. [26] and is beyond the scope of this paper. As discussed in Section 4.2.2, the target normal load provided by the friction bolt was 50 kN and the bolt load of the friction bolt was monitored using the through-hole bolt load cell throughout the test. Between tests, the friction bolt was retightened to the target normal load level if bolt load loss was observed.

Figure 13 presents selected results of Test Group 2. The force-displacement response of the friction-based connection was plotted for tests having expected seismic-induced responses as the input excitation. It is observed that under earthquake-type input excitation, the proposed friction-based connection exhibited a stable force-displacement response that could be idealized as a Coulomb-type frictional behavior. Comparing Test 1 with Test 14, Test 2 with Test 15, and Test 3 with Test 13, noticeable difference in the magnitude of the connection sliding force can be observed. Figure 14 presents the evolution of the magnitude of the connection sliding force with respect to the cumulative displacement that the friction interface of the connection underwent. In Figure 14, different tests are separated by vertical dashed lines. The bolt load variation, defined as the relative difference between the bolt load at the beginning and at the end of the test, is plotted in the same figure. A negative bolt load variation means that there was a bolt load loss in this test. Figure 14 shows that at the beginning of the test when the cumulative displacement was relatively small, the connection sliding force

10969845, 2026, 6, Downloaded from https://onlinelibrary.wiley.com/doi/10.1002/eqe.70121 by University Of California, Wiley Online Library on [07/11/2026]. See the Terms and Conditions (https://onlinelibrary.wiley.com/terms-and-conditions) on Wiley Online Library for rules of use; OA articles are governed by the applicable Creative Commons License

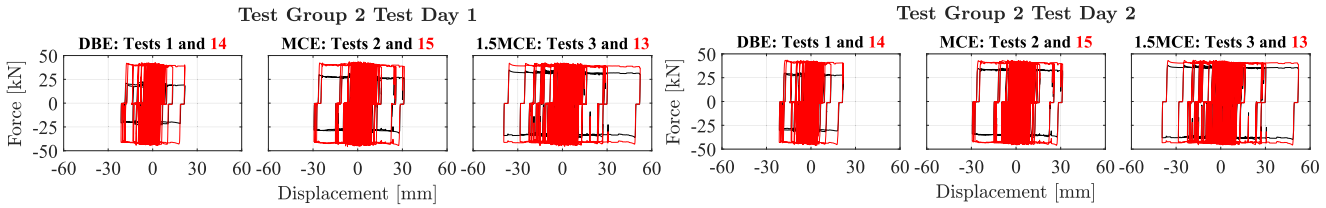


FIGURE 13 | Selected results of Test Phase 1 Test Group 2: force-displacement responses of the connection under earthquake-type input excitation (Tests 1, 2, 3, 13, 14, and 15).

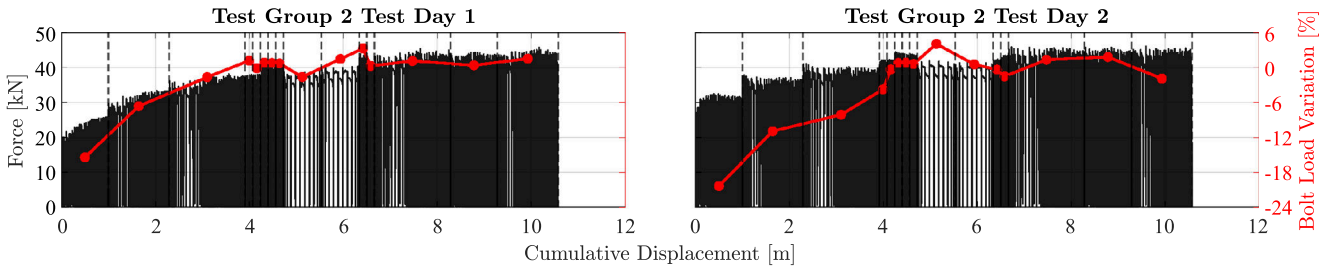


FIGURE 14 | Results of Test Phase 1 Test Group 2: evolution of the connection force with respect to the cumulative displacement and the variation of the bolt load in each test (tests are separated using dashed lines).

was lower than the target connection sliding force (40 kN). As the cumulative displacement increased, the connection sliding force increased and reached a relatively constant level equal to the target connection sliding force. Moreover, it is observed that the bolt load loss was more significant at the beginning of the test and was reduced as the cumulative displacement increased.

The observed evolution of the connection force and the bolt load variation with respect to the cumulative displacement of the friction interface was attributed to the break-in effect of the friction interface. When two surfaces are first brought into contact under the normal load and start sliding relative to each other, the break-in process happens. Changes in the coefficient of friction and the wear rate of a friction interface usually happen at this stage due to changes in the surface conditions [56]. The break-in process depends on the cumulative displacement and as the cumulative displacement increases, the response of the friction interface will reach a relatively steady state [56], in which the coefficient of friction and the wear rate will reach a relatively constant level. Chen et al. [26] studied the break-in effect of composite-metallic friction interfaces for earthquake engineering applications. For the Gatke 398 to low-carbon structural steel friction interface used in this study, the break-in effect was attributed to the wearing of surface asperities and an increase in the adhesive friction at the beginning of sliding, and as a result, the friction interface exhibited an increase in the coefficient of friction upon reaching the steady state. This explains the evolution of the connection sliding force observed in Figure 14. In addition, Chen et al. [26] showed that due to the break-in effect, composite metallic friction interfaces have a higher wear rate at the beginning of sliding. A higher wear rate increases the wear volume, causing the friction shims to be thinner, and consequently causing a shortening of the friction bolt and inducing a higher bolt load loss at the beginning of sliding. As the cumulative displacement increased, the wear rate was reduced; therefore, the increase in the wear volume became slower and as a result, the induced bolt load loss became lower. This explains the evolution of the bolt load variation observed in Figure 14. The break-in effect observed in Test Group 2 highlighted the importance of breaking in the friction shims before installing the connection onto the structure, so that the friction interface of the connection can reach a relatively steady state and the connection can generate a relatively constant connection sliding force with a relatively low bolt load loss.

As observed in Figure 14, at a cumulative displacement of about 4 meters, the connection sliding force reached a relatively constant level and the bolt load variation was effectively close to zero. Based on this result, a break-in loading protocol as shown in Figure 15 was proposed for the friction-based connection in this study. The proposed break-in loading protocol consisted of three sets of break-in tests having ramped sinusoidal waves as the imposed displacement time history of the input excitation. Between the break-in tests and at the end of the break-in loading protocol, the friction bolt was retightened to the original target bolt load if bolt load loss was observed. The peak sliding velocity imposed by the proposed break-in loading protocol was 7.62 mm/s. The total cumulative displacement imposed by the proposed break-in loading protocol was 4 meters. Note that this proposed break-in loading protocol was developed for the specific material pair (composite material Gatke 398 in contact with low-carbon structural steel) used in the friction interface for this connection, and for a specific normal pressure level (for the connection tested, the target normal load was 50 kN and the resulting target nominal normal pressure was 3.8 MPa). If the material pair for the friction interface is different or if a different normal pressure is applied, the break-in loading protocol may need to be revised accordingly [26].

Following Test Group 2, Test Group 3 was conducted to verify the proposed break-in loading protocol in Figure 15. Table 4 presents the loading protocol of Test Group 3. Tests 1, 2, and 3 were

10969845, 2026, 6, Downloaded from https://onlinelibrary.wiley.com/doi/10.1002/eqe.70121 by University Of California, Wiley Online Library on [07/11/2026]. See the Terms and Conditions (https://onlinelibrary.wiley.com/terms-and-conditions) on Wiley Online Library for rules of use; OA articles are governed by the applicable Creative Commons License

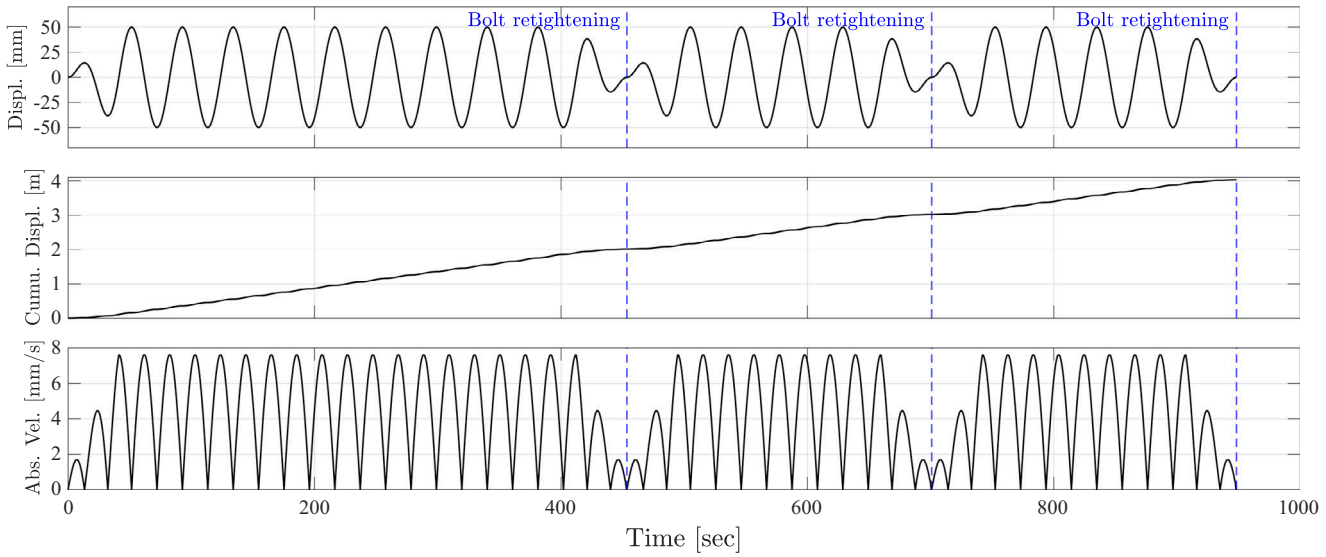


FIGURE 15 | Proposed break-in loading protocol for the friction-based connection in this study. From top to bottom: imposed displacement time history; cumulative displacement time history; absolute sliding velocity time history.

TABLE 4 | Loading protocol of Test Group 3.

Test ID	Input type	Peak displ. [mm]	Peak vel. [mm/sec]	Descriptions
1	Ramped sine	50	7.6	Break-in test one to establish the break-in effect
2	Ramped sine	50	7.6	Break-in test two to establish the break-in effect
3	Ramped sine	50	7.6	Break-in test three to establish the break-in effect
4	EQ-DBE	22	~28	Post-break-in-process assessment of the connection response at DBE level earthquake
5	EQ-MCE	31	~35	Post-break-in-process assessment of the connection response at MCE level earthquake
6	EQ-1.5MCE	52	~36	Post-break-in-process assessment of the connection response at 1.5 × MCE level earthquake

break-in tests following the break-in loading protocol in Figure 15. Tests 4, 5, and 6 were follow-up tests with expected seismic-induced responses as the displacement histories of the input excitation. Following the break-in loading protocol in Figure 15, the friction bolt was retightened to the target normal load level (50 kN) between Tests 1 and 2, Tests 2 and 3, and after the completion of Test 3, if bolt load loss was observed. Figure 16a presents the force-displacement response of the connection in Test Group 3. It can be observed that the connection generated a lower sliding force in Test 1 and the connection sliding force increased in Tests 2 and 3 as the break-in effect was established. In Tests 4, 5, and 6, the connection sliding force was maintained at a relatively constant level of about 40 kN. Figure 16b presents the time histories of the imposed displacement, the recorded connection sliding force and the bolt load, and the computed coefficient of friction μ_{computed}. Upon the establishment of the break-in effect after Test 3, the coefficient of friction of the sliding interface reached a relatively constant level. Hence, Test Group 3 verified the effectiveness of the proposed break-in loading protocol.

4.2.5 | Summary of Test Phase 1 Results

Throughout a series of component-level connection tests, Test Phase 1 showed that the proposed friction-based connection exhibited a stable force-displacement response that could be idealized as a Coulomb-type frictional behavior under different loading conditions and for various force demands. Furthermore, it demonstrated that by using the novel design concept with loose steel washer plates, the stable Coulomb-type frictional behavior

10969845, 2026, 6, Downloaded from https://onlinelibrary.wiley.com/doi/10.1002/eqe.70121 by University Of California, Wiley Online Library on [07/11/2026]. See the Terms and Conditions (https://onlinelibrary.wiley.com/terms-and-conditions) on Wiley Online Library for rules of use; OA articles are governed by the applicable Creative Commons License

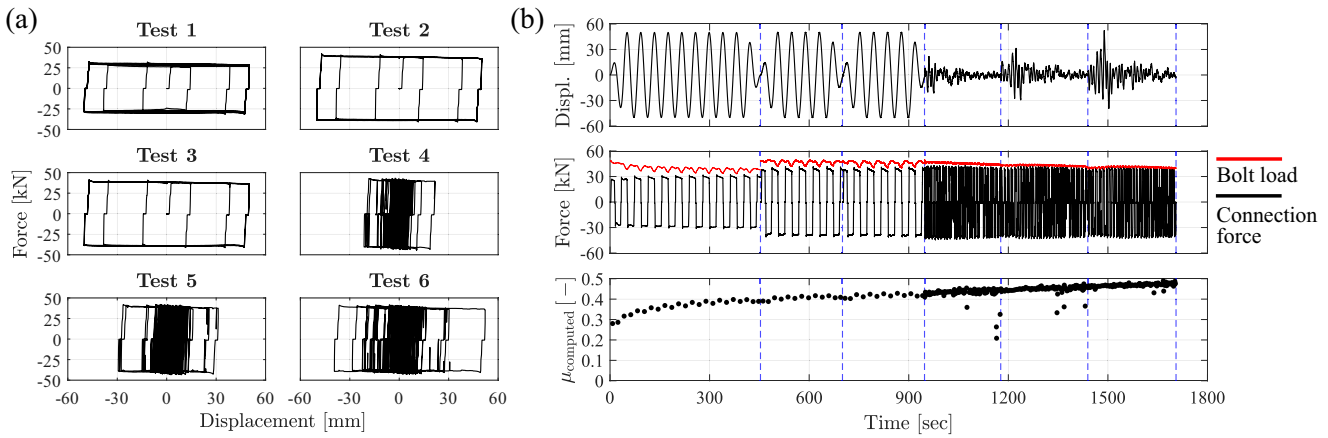


FIGURE 16 | Results of Test Phase 1 Test Group 3: (a) Force-displacement responses of the connection in Test Group 3 and (b) Time history results of Test Group 3 (tests are separated by dashed blue lines). From top to bottom: imposed displacement time history; recorded connection sliding force and bolt load time histories; computed coefficient of friction $\mu_{computed}$ time history.

could be achieved without enforcing tight geometric tolerances when machining the parts. Test Phase 1 also highlighted that the break-in effect of the composite-metallic friction interface influenced the early-stage response of the friction-based connection. After the break-in effect was established, the connection exhibited a relatively constant connection sliding force and a relatively low bolt load loss. Based on these results, a break-in loading protocol was proposed and verified for use in Test Phase 2 shaking table tests so that breaking in of the friction shims could be performed before installing the friction-based connections onto the structure.

4.3 | Test Phase 2: Shaking Table Test

Test Phase 2 was a shaking table test conducted at NCREE in Taiwan, in which a full-scale three-story, re-centering steel braced frame with sliding slabs was tested. In this frame specimen, the proposed friction-based connection was used as the force-limiting connection to limit the force transferred between the sliding slabs and the steel frame. Spring devices were used with friction-based connections in the frame specimen; they were designed to provide the re-centering capability when the slabs moved. Shaking table tests results demonstrated that, compared with the conventional frame design, the frame specimen incorporating friction-based force-limiting connections, spring devices, and sliding slabs exhibited reduced slab acceleration, roof frame drift, and base shear demands, and thereby having the potential to limit damage to nonstructural components and to support the objective of post-earthquake functional recovery [45]. The detailed discussion about the design of the re-centering braced frame, the test setup, and the test response of the frame specimen and the spring devices, can be found in Chou et al. [45]. Only basic information about the shaking table test is provided in Section 4.3.1 to facilitate follow-up discussions. In contrast, this paper focuses specifically on the friction-based connection used in this shaking table test, including its installation process, the instrumentation plan, and the connection response throughout the pre-shaking-table-test preparation, the shaking table test, and the post-shaking-table-test evaluation.

4.3.1 | Shaking Table Test Setup

Figure 17a presents an overview of the re-centering steel frame specimen that had three stories. The sliding slabs were termed based on the story above it; from top to bottom, they were termed RFL, 3FL, and 2FL. At each story, two friction-based connections were used to transfer the force between the steel frame and sliding slabs. They were placed on the west and east side of the steel beams of the lateral force resisting system (LFRS). The friction-based connection was termed based on the sliding slab to which it was connected and its reference position with respect to the steel beam. For example, the friction-based connection 3FL-W represented the friction-based connection connecting to the Sliding slab (3FL) and was installed on the west side of the steel beam in the LFRS system. Six friction-based connections were used in this frame (i.e., friction-based connections RFL-W/E, 3FL-W/E, and 2FL-W/E). For RFL and 3FL friction-based connections, the target connection sliding force was 40 kN; for 2FL friction-based connections, the target connection sliding force was 20 kN. The shaking table tests were conducted along the north-south direction of the frame (i.e., the motion was one-dimensional); therefore, the friction-based connections were also oriented in the north-south direction.

4.3.2 | Installation of the Connection Onto the Frame Specimen

Figure 18 demonstrates the installation process of the friction-based connection onto the steel frame specimen. In the shaking table test setup, the sliding end of the connection was connected to the steel beam, while the fixed end of the connection was connected to the concrete sliding slab. Steel connection plates were used on both ends of the friction-based connection to connect the ends of the connection with the steel beam and the sliding slab, as shown in Figure 18. To install the connection, first the connection was lifted roughly to its designated position by a crane. After aligning one bolt hole on the sliding end with the connection plate, a bolt was inserted to temporarily connect the sliding end with the connection plate and the inserted bolt was also used as a temporary pivot point, as shown in Figure 18. The

10969845, 2026, 6, Downloaded from https://onlinelibrary.wiley.com/doi/10.1002/eqe.70121 by University Of California, Wiley Online Library on [07/11/2026]. See the Terms and Conditions (https://onlinelibrary.wiley.com/terms-and-conditions) on Wiley Online Library for rules of use; OA articles are governed by the applicable Creative Commons License

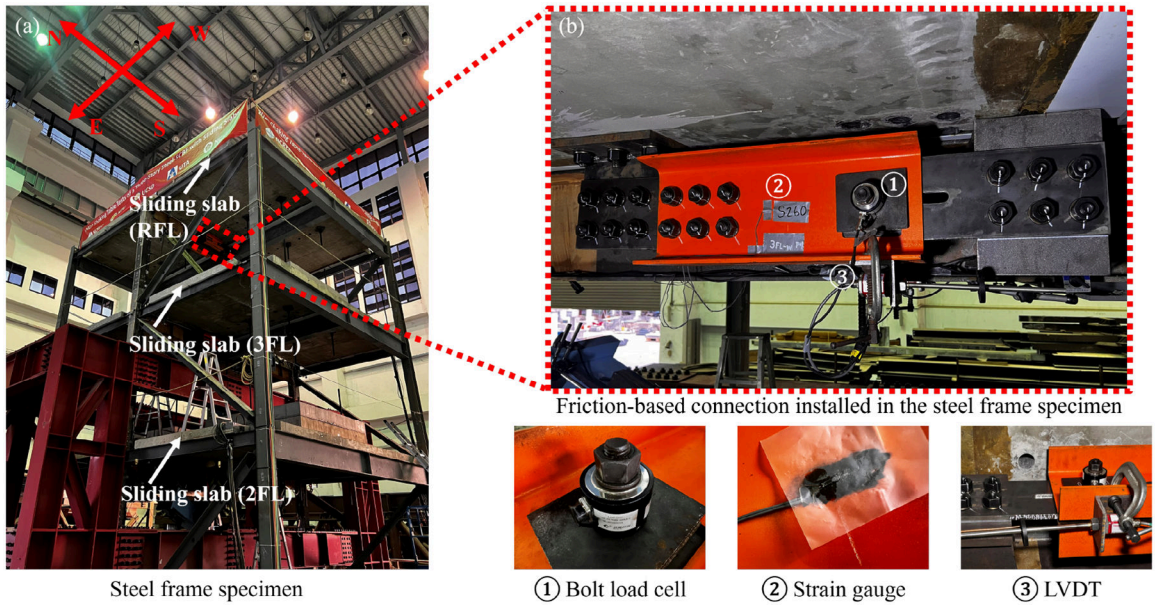


FIGURE 17 | Test Phase 2 shaking table test (a) Overview of the steel frame specimen and (b) Instrumentation related to the friction-based connection.



FIGURE 18 | Demonstration of the connection installation process.

connection was then rotated about this pivot point to align the bolt holes on the fixed end with its corresponding steel connection plate. Once aligned, a temporary fixing tool was placed on the fixed end to hold the connection in position. At this stage, the bolt holes on both ends were properly aligned and the connection was in its designated position. The final step was to insert all the bolts on both ends and to tighten the bolts so that the friction-based connection was properly connected with the connection plates. In this test, the connecting bolts on both ends were tightened to a slip-critical condition. Figure 18 also presents the final state of the installation process when the connection was installed on the frame specimen. The entire installation process was completed by three workers, taking approximately eight to twelve minutes.

4.3.3 | Instrumentation

Figure 17b presents the instrumentation setup for the friction-based connection in Test Phase 2 shaking table tests. Three types of instruments were used for the friction-based connection. The bolt load cell was used to monitor the load variation of the friction bolt throughout the shaking table test. A linear variable differential transformer (LVDT) was used to measure the connection displacement. Strain gauges were mounted on both steel channels of the connection as an indirect method for estimating the connection force. However, this approach was later found to be unreliable due to difficulties in accurately calibrating the relationship between the measured strain and the actual connection force. In addition, some strain gauges might become

10969845, 2026, 6, Downloaded from https://onlinelibrary.wiley.com/doi/10.1002/eqe.70121 by University Of California, Wiley Online Library on [07/11/2026]. See the Terms and Conditions (https://onlinelibrary.wiley.com/terms-and-conditions) on Wiley Online Library for rules of use; OA articles are governed by the applicable Creative Commons License

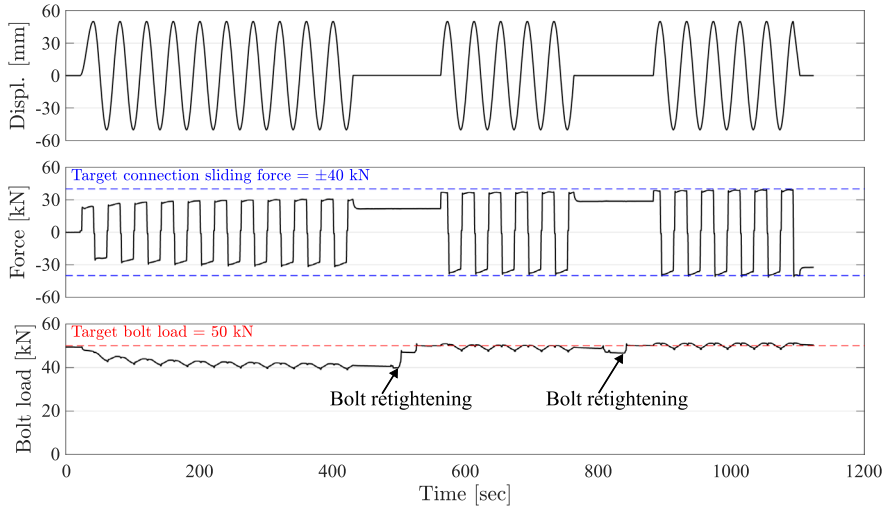


FIGURE 19 | Selected results of Test Phase 2 Test Group 1 of one representative connection. From top to bottom: imposed displacement time history; connection sliding force time history; and friction bolt load time history.

TABLE 5 | Testing sequence of the shaking table test.

Test	Test intensity	PGA [g]	Test	Test intensity	PGA [g]
1	6% DBE	−0.02	5	98% MCE	−0.32
2	35% DBE	−0.08	6	−120% MCE	0.38
3	70% DBE	−0.17	7	166% MCE	0.53
4	92% DBE	−0.22	8	−161% MCE	−0.51

loose and slipped relative to the steel channel during the test, resulting in measurement errors.

4.3.4 | Results

Before installing six friction-based connections onto the frame specimen, all connections underwent the break-in loading protocol proposed in Test Phase 1 (Figure 15) as the pre-shaking-table-test preparation step and this was denoted as Test Phase 2 Test Group 1. Figure 19 presents the result of one of the connections. It can be observed that towards the end of the break-in loading protocol, the connection sliding force increased to the target connection sliding force (±40 kN) and the sliding force was maintained at a relatively constant level. In addition, the bolt load loss of the friction bolt decreased as the break-in process continued. Although not shown, the testing results of the other five connections were similar. The six friction-based connections after the break-in process in Test Phase 2 Test Group 1 were considered ready for the shaking table tests in Test Group 2.

In the shaking table test (Test Phase 2 Test Group 2), the selected ground motion was obtained from the September 18, 2022, Guanshan and Chihshang Earthquake, which was recorded at the EYUL-EW station close to a collapsed building [57]. Eight tests were conducted with ground motions having different intensities by scaling the peak ground acceleration (PGA). Table 5 presents the testing sequence of the shaking table test. The test intensity was obtained by normalizing the measured PGA of the shaking table platen to the design PGA at the DBE level (0.24 g) and the MCE level (0.32 g). The measured PGA of the shaking table platen is also presented in Table 5. Between tests, the specimen was inspected to assess the condition of all members including beams, columns, braces, and friction-based connections; no additional actions (e.g., retightening the friction bolts) were performed.

Figure 20 shows the measured displacement time history, the cumulative displacement time history, and the absolute sliding velocity time history of the RFL-W and RFL-E friction-based connections throughout the shaking table test. The responses of the RFL friction-based connections were of interest because they had higher peak displacement demands than the 3FL and 2FL friction-based connections. From Figure 20, it is observed that since the shaking table test motion was along the plane of the LFRS (north-south direction) and given that the steel frame specimen was essentially symmetric about the north-south axis, RFL-W and RFL-E friction-based connections had nearly identical responses.

The displacement time history shows that during Tests 1 and 2 (6% DBE and 35% DBE), there was negligible relative displacement on the sliding ends of the connections. The connection displacement became noticeable from Test 3 (70% DBE) afterward. A peak connection displacement of -69.2 mm was observed in Test 7 (166% MCE). Due to the re-centering mechanism of the frame and the slabs, the residual displacement of the connection after each test remained relatively small, consistently less than 6 mm. The cumulative displacement time history was derived from the recorded connection displacement time history. The cumulative displacement time history started from 4.1 m to take into account the cumulative displacement of the friction interface during the pre-shaking-table-test break-in process in Test Group 1. The cumulative displacement time history confirmed the previous observation that the connection displacement was negligible in Tests 1 and 2 and became noticeable from Test 3 afterward. The total cumulative displacement of eight tests was approximately 0.85 m for RFL connections. The absolute sliding velocity time

10969845, 2026, 6, Downloaded from https://onlinelibrary.wiley.com/doi/10.1002/eqe.70121 by University Of California, Wiley Online Library on [07/11/2026]. See the Terms and Conditions (https://onlinelibrary.wiley.com/terms-and-conditions) on Wiley Online Library for rules of use; OA articles are governed by the applicable Creative Commons License

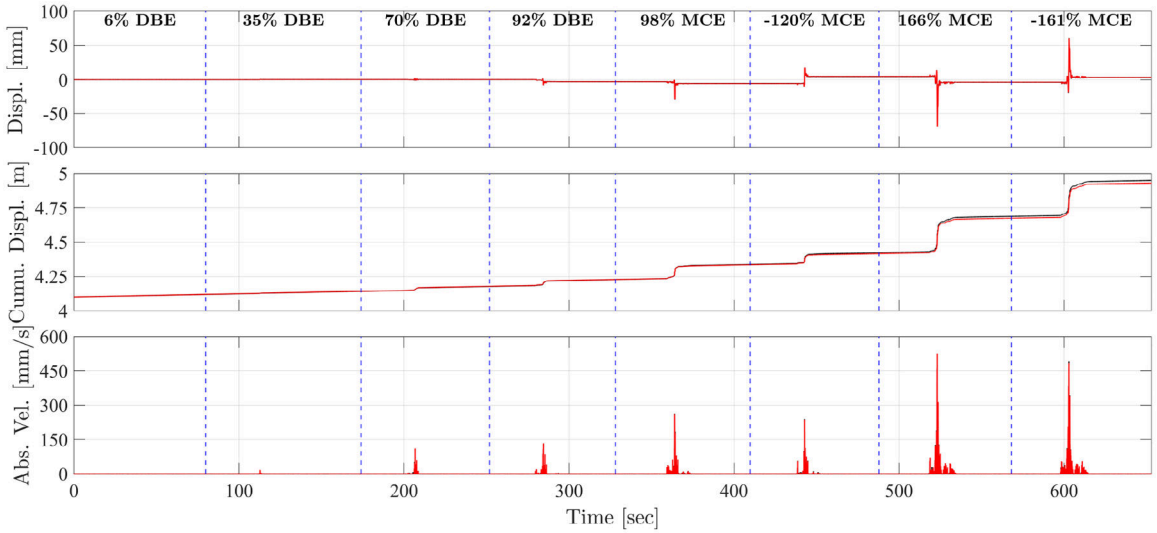


FIGURE 20 | Selected results of the shaking table test: displacement time history, cumulative displacement time history, and absolute sliding velocity time history of RFL-W (in black) and RFL-E (in red) friction-based connections.

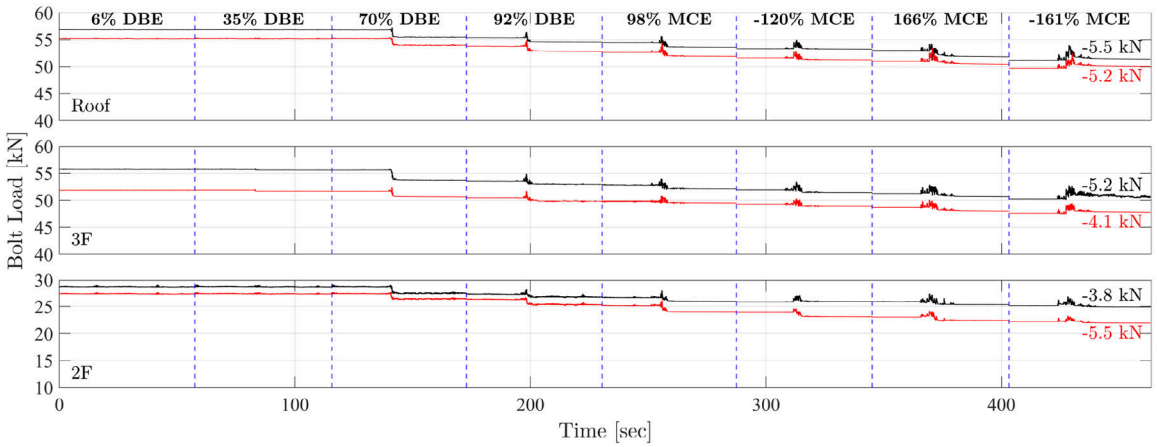


FIGURE 21 | Friction bolt load time history of all the friction-based connections in this frame specimen throughout the shaking table test. From top to bottom: friction bolts for RFL connections, for 3FL connections, and for 2FL connections. Responses in black are for -W connections and responses in red are for -E connections.

history was also derived from the recorded connection displacement time history. The peak absolute sliding velocity that the connection underwent throughout the shaking table test was observed in Test 7 (166% MCE), of approximately 525 mm/s.

Figure 21 presents the friction bolt load time history of all the friction-based connections in the frame specimen. The difference in recorded testing durations between the bolt load time history in Figure 21 and the displacement time history in Figure 20 was attributed to the use of separate data acquisition channels for LVDTs and bolt load cells. The data acquisition channels for these two instruments were started and stopped at different times, resulting in a difference in the recorded testing durations. The displacement response and the friction bolt load time history were processed separately, and no synchronization was performed. As shown in Figure 21, the bolt load variation during Tests 1 and 2 was negligible. The first noticeable bolt load loss occurred in Test 3. A possible explanation for the observed bolt load loss in Test 3 was that, as shown in Figure 20, the connection displacement became noticeable in Test 3, which means that the steel channel made contact with the friction shim, pushed the friction shim to move relative to the internal sliding plate, and activated the sliding friction mechanism. During the assembly process, when the friction shim was placed into the opening of the steel channel, it was possible that the edge of the friction shim was not perfectly aligned with the edge of the opening of the steel channel. The contact between the steel channel and the edge of the friction shim potentially created a self-aligning mechanism and forced the edge of the friction shim to align with the edge of the opening of the steel channel. This process potentially induced a slight in-plane rotation of the friction shim and might consequently result in the observed bolt load loss in Test 3. The cumulative bolt load loss from the beginning to the end of the testing sequence is also reported in Figure 21 for each connection. For all the connections, the amount of the bolt load loss at the end of the testing sequence was similar, being about 5 kN. The cumulative bolt load loss throughout the testing sequence was primarily attributed to the wear of the friction shims [26].

10969845, 2026, 6, Downloaded from https://onlinelibrary.wiley.com/doi/10.1002/eqe.70121 by University Of California, Wiley Online Library on [07/11/2026]. See the Terms and Conditions (https://onlinelibrary.wiley.com/terms-and-conditions) on Wiley Online Library for rules of use; OA articles are governed by the applicable Creative Commons License

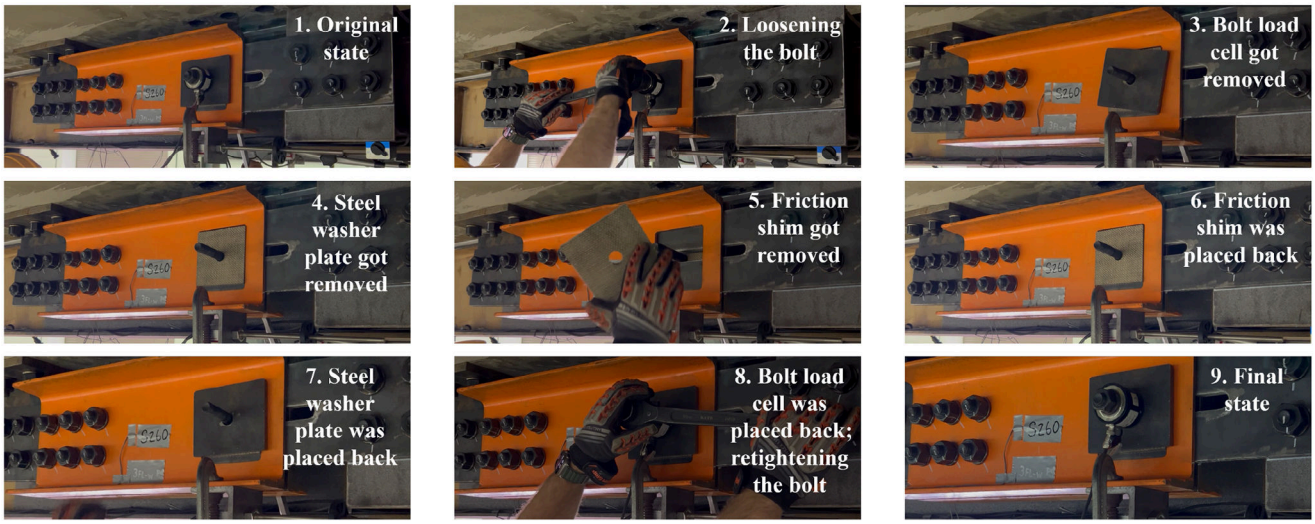


FIGURE 22 | Friction shim replacement demonstration after the the completion of the shaking table tests while the friction-based connection remained installed on the frame specimen.

Although there was no observed mechanical failure or damage associated with the Gatke 398 friction shims, the replacement of friction shims was still demonstrated after the completion of all shaking table tests, while the friction-based connection remained installed on the frame specimen. This was to experimentally justify the advantage of the design concept of this connection, that the design with loose steel washer plates allows quick inspection and replacement of the friction shims. Figure 22 presents the friction shim replacement process. To replace the friction shims, the friction bolt was first loosened. Then the bolt load cell and the steel washer plate were removed, making the friction shim exposed. The friction shim could then be removed from the connection for inspection, and could be replaced if necessary. After placing the friction shim back to the connection, the steel washer plate and the bolt load cell were placed back. The friction bolt was then retightened to the designed normal load level to complete the assembly process. The entire friction shim replacement process was completed by two workers and took approximately three minutes.

The limitation of Test Group 2 was that the use of strain gauges as an indirect measurement for estimating the connection force was found to be unreliable for estimating the force response of the connection during shaking table tests. To address this limitation, follow-up connection tests were conducted in Test Group 3 as a post-shaking-table-test evaluation process to provide a supporting evidence of the response of the connection during the shaking table tests. In Test Group 3, one of the friction-based connections with a target connection sliding force of 40 kN was removed from the steel frame specimen and was subjected to six displacement-controlled cyclic tests to verify the connection response during the shaking table test. Out of the six tests, one test had linear ramped waves as the imposed displacement time history of the input excitation while the remaining five tests used recorded connection displacement responses from Tests 4 to 8 in the shaking table test as the imposed displacement time history of the input excitation. The recorded connection displacement responses used were from an RFL friction-based connection.

Figure 23 presents the force-displacement response of the connection in Test Group 3. It is observed that in the six tests conducted in Test Group 3, the friction-based connection exhibited a stable force-displacement response and the connection sliding force was maintained at a relatively constant level of about 40 kN. Hence, the results of Test Group 3 provided supporting evidence that the force-displacement response of the connection was stable throughout the shaking table test.

Approximately ten months after the shaking table test, Test Group 4 was conducted to investigate the possible influence of environmental exposure and aging effects on the response of the friction-based connection. During the period between the shaking table test and Test Group 4, the connection specimen was stored in the lab without any protection. The friction bolt was hand-tightened during the storage process and was retightened to the target normal load level of 50 kN before the start of Test Group 4. In Test Group 4, two tests were conducted. Both tests used linear ramped waves as the imposed displacement time history of the input excitation. Figure 24 presents the force-displacement response of the connection in Test Group 4. The results showed that the friction-based connection exhibited a stable force-displacement response and the connection sliding force was maintained at a relatively constant level of about 40 kN.

4.3.5 | Summary of Test Phase 2 Results

Test Phase 2 successfully implemented the use of the proposed friction-based connection in the three-story re-centering steel frame specimen for the shaking table test. The connection successfully accommodated a relative displacement of approximately 70 mm between the steel frame and the sliding slab. The bolt load loss of the friction bolt of the connection was relatively low. The repairability of the connection was demonstrated by replacing the friction shims while the friction-based connection remained installed on the frame specimen. The pre-shaking-table-test preparation and post-shaking-table-test evaluation tests further demonstrated that after the break-in effect was established, the

10969845, 2026, 6, Downloaded from https://onlinelibrary.wiley.com/doi/10.1002/eqe.70121 by University Of California, Wiley Online Library on [07/11/2026]. See the Terms and Conditions (https://onlinelibrary.wiley.com/terms-and-conditions) on Wiley Online Library for rules of use; OA articles are governed by the applicable Creative Commons License

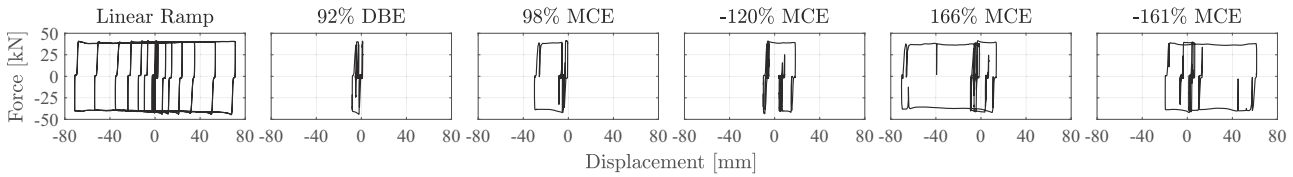


FIGURE 23 | Force-displacement responses of the connection in Test Phase 2 Test Group 3.

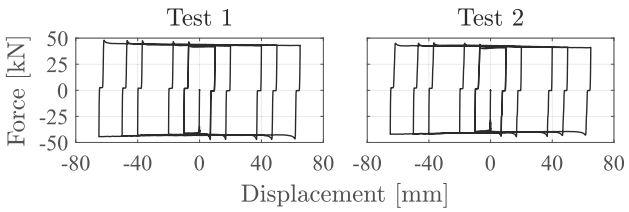


FIGURE 24 | Force-displacement responses of the connection in Test Phase 2 Test Group 4.

connection exhibited a stable force-displacement response and the connection sliding force was relatively constant. Test Group 4 results indicated that ten months of storage had no noticeable impact on the force-displacement response of the connection, which enhanced the confidence in the long-term performance of the proposed friction-based connection.

5 | Conclusions

This paper presents the development and experimental characterization of a novel yet practical design concept for friction-based structural components intended for the use as energy dissipation devices or force-limiting connections in earthquake-resistant structures. The proposed connection has a slotted-bolted configuration and the main difference between this design and the conventional design of slotted-bolted friction-based components is that, in this design, initially loose plates are used to establish the clamping mechanism. This design concept offers two key advantages. Firstly, The connection has stable force-displacement responses and generates relatively constant sliding forces without enforcing tight geometric tolerances in the machining of the parts. Secondly, the design with loose steel washer plates allows quick inspection and replacement of friction shims if needed.

To verify this design concept, a numerical simulation was conducted to assess the expected kinematics and force-displacement responses of the connection. Critical regions of high stress were identified to facilitate the design and detailing of the parts. A friction-based structural component, which has a required sliding force of 40 kN, was designed with the proposed design concept and tested. Two test phases including component-level connection tests (116 tests in total) and a full-scale shaking table test of a three-story re-centering steel braced frame (8 tests in total), in which the proposed friction-based connection was designed as the force-limiting connection between the steel frame and the sliding slab, were performed. Based on the results of the experimental study, the following conclusions were made:

- Without enforcing tight geometric tolerances in the machining of the parts, the friction-based force-limiting connection designed with loose steel washer plates exhibited stable force-displacement responses. The connection tested in this study generated a relatively constant sliding friction force equal to the required sliding force (40 kN) without exhibiting the uncontrolled displacement-dependent variable friction force. Hence, it was demonstrated that compared with the conventional design of slotted-bolted friction-based components, the proposed design concept with loose steel washer plates can save both manufacturing time and cost.
- The break-in effect of the composite-metallic friction interface influenced the early-stage response of the friction-based connection. It is recommended to break in the composite friction shim before installing the connection onto the structure so that the friction interface of the connection can reach a relatively steady state and the connection can generate a relatively constant connection sliding force with a relatively low bolt load loss.
- For the connection tested in this study (friction interface: Gatke 398 to low-carbon structural steel; nominal normal pressure: 3.8 MPa), the break-in loading protocol used was the following: Break-in test 1 (ramped sinusoidal waves with a cumulative displacement of 2 meters) → Bolt retightening → Break-in test 2 (ramped sinusoidal waves with a cumulative displacement of 1 meter) → Bolt retightening → Break-in test 3 (ramped sinusoidal waves with a cumulative displacement of 1 meter) → Bolt retightening. The ramped sinusoidal waves used had a peak displacement of 50.8 mm and a peak sliding velocity of 7.62 mm/s. The break-in loading protocol resulted in a total cumulative displacement of 4 meters.
- Throughout the shaking table test, the proposed friction-based connection successfully accommodated a relative displacement of approximately 70 mm between the steel frame and the sliding slab, under a peak sliding velocity of approximately 525 mm/s, with a relatively low bolt load loss (5 kN).
- The inspection and replacement of the friction shims for the friction-based connection designed with loose steel washer plates could be performed relatively easily without removing the connection from the structure. Compared with the conventional design, of which the inspection and replacement process requires removal of external clamping plates, the proposed design concept with loose steel washer plates allows a quicker inspection and repairing process, which potentially enhances the practicality of the connection in real applications and supports the long-term functionality of earthquake-resistant buildings equipped with friction-based connections.
- The two test phases showed no failure or damage in the parts of the proposed friction-based components even after multiple displacement time histories.

10969845, 2026, 6, Downloaded from https://onlinelibrary.wiley.com/doi/10.1002/eqe.70121 by University Of California, Wiley Online Library on [07/11/2026]. See the Terms and Conditions (https://onlinelibrary.wiley.com/terms-and-conditions) on Wiley Online Library for rules of use; OA articles are governed by the applicable Creative Commons License

- Reference times for manufacturing, assembling, installing, and repairing of one connection are as follows: Manufacturing: 180 minutes; Assembling: 3 minutes; Installing: 8–12 minutes; Repairing: 3 minutes.

In conclusion, the proposed design concept with loose steel washer plates provides a low-cost, less sensitive to machining tolerances, and easily repairable solution for designing friction-based structural components in earthquake engineering applications. Potential future work includes (1) component-level connection tests under higher required sliding forces and (2) system-level shaking table tests for structures equipped with the proposed connection under multi-directional seismic excitation.

Author contributions

Kaixin Chen: writing – original draft and editing, Visualization, Experiments, Data curation and analysis, Methodology, Investigation. **Georgios Tsampras:** writing – original draft and editing, Research need and scope conceptualization, Friction-based connection design concept, manufacturing and experiments, Resources, Funding acquisition and project administration (UC San Diego), Methodology, Investigation, Data curation and analysis. **Chung-Che Chou:** writing – review and editing, Resources, Experiments, Resources, Funding acquisition and project administration (NCREE), Methodology, Investigation, Sliding floor shake table testing lead, Shake table testing data curation. **Huang-Zuo Lin:** writing – review, Experiments, Data curation, Methodology, Investigation. **Chi-Jeng Wu:** writing – review, Experiments, Data curation, Methodology, Investigation. **Alvaro Córdova:** writing – review, Experiments, Data curation, Methodology, Investigation. **Chia-Ming Uang:** writing – review and editing, Sliding floor design conceptualization, Methodology, Investigation. **Shih-Ho Chao:** writing – review and editing, Sliding floor design conceptualization, Methodology, Investigation.

Acknowledgments

The authors are grateful for financial support provided by UC San Diego Structural Engineering Distinguished Fellowship, the Western Steel Council, and the Department of Structural Engineering at UC San Diego. Composite friction materials donated by ScanPac Mfg., Inc. are appreciated. The shaking table tests of the three-story recentering braced frame at National Center for Research on Earthquake Engineering (NCREE) were supported by the National Science and Technology Council under the project NSTC No. 112-2625-M-002-019 and the National Applied Research Laboratories in Taiwan. The technical support from the laboratory staff at NCREE is appreciated. Any opinions, findings, and conclusions expressed in this paper are those of the authors and do not necessarily reflect the views of the parties acknowledged here.

Conflicts of Interest

The authors declare no conflicts of interest.

Data Availability Statement

Data will be made available upon reasonable request.

References

1. G. Tsampras, "Force-Limiting Floor Diaphragm Connection for Earthquake-Resistant Buildings," Ph.D. dissertation, (Lehigh University, 2016), https://preserve.lehigh.edu/etd/2851.

2. G. Tsampras, R. Sause, D. Zhang, et al., "Development of Deformable Connection for Earthquake-Resistant Buildings to Reduce Floor Accelerations and Force Responses," *Earthquake Engineering & Structural Dynamics* 45, no. 9 (2016): 1473–1494, https://doi.org/10.1002/eqe.2718.

3. G. Tsampras, R. Sause, R. B. Fleischman, and J. I. Restrepo, "Experimental Study of Deformable Connection Consisting of Friction Device and Rubber Bearings to Connect Floor System to Lateral Force Resisting System," *Earthquake Engineering & Structural Dynamics* 47, no. 4 (2018): 1032–1053, https://doi.org/10.1002/eqe.3004.

4. M. Paronesso and D. G. Lignos, "Seismic Design and Performance of Steel Concentrically Braced Frame Buildings With Dissipative Floor Connectors," *Earthquake Engineering & Structural Dynamics* 51, no. 15 (2022): 3505–3525, https://doi.org/10.1002/eqe.3733.

5. T. T. Soong and G. F. Dargush, *Passive Energy Dissipation Systems in Structural Engineering* (Wiley, 1997).

6. B. G. Morgen and Y. C. Kurama, "Seismic Response Evaluation of Posttensioned Precast Concrete Frames With Friction Dampers," *Journal of Structural Engineering* 134, no. 1 (2008): 132–145, https://doi.org/10.1061/(ASCE)0733-9445(2008)134:1(132).

7. L.-L. Song, T. Guo, and C. Chen, "Experimental and Numerical Study of a Self-Centering Prestressed Concrete Moment Resisting Frame Connection With Bolted Web Friction Devices," *Earthquake Engineering & Structural Dynamics* 43, no. 4 (2014): 529–545, https://doi.org/10.1002/eqe.2358.

8. M. N. Eldin, A. J. Dereje, and J. Kim, "Seismic Retrofit of RC Buildings Using Self-Centering PC Frames With Friction-Dampers," *Engineering Structures* 208 (2020): 109925, https://doi.org/10.1016/j.engstruct.2019.109925.

9. T. Fitzgerald, T. Anagnos, M. Goodson, and T. Zsutty, "Slotted Bolted Connections in Aseismic Design for Concentrically Braced Connections," *Earthquake Spectra* 5, no. 2 (1989): 383–391, https://doi.org/10.1193/1.1585528.

10. R. Tremblay, "Seismic Behavior and Design of Friction Concentrically Braced Frames for Steel Buildings," Ph.D. dissertation, (The University of British Columbia, 1993), https://dx.doi.org/10.14288/1.0050464.

11. H.-H. Khoo, C. Clifton, G. MacRae, H. Zhou, and S. Ramhormozian, "Proposed Design Models for the Asymmetric Friction Connection," *Earthquake Engineering & Structural Dynamics* 44, no. 8 (2015): 1309–1324, https://doi.org/10.1002/eqe.2520.

12. V. Piluso, G. Rizzano, R. Montuori, et al., *Free From Damage Steel Connections* (Publication office of the European Union, 2019).

13. A. Filiatrault, "Analytical Predictions of the Seismic Response of Friction Damped Timber Shear Walls," *Earthquake Engineering & Structural Dynamics* 19, no. 2 (1990): 259–273, https://doi.org/10.1002/eqe.4290190209.

14. W. Y. Loo, C. Kun, P. Quenneville, and N. Chouw, "Experimental Testing of a Rocking Timber Shear Wall With Slip-Friction Connectors," *Earthquake Engineering & Structural Dynamics* 43, no. 11 (2014): 1621–1639, https://doi.org/10.1002/eqe.2413.

15. Z. Li, F. Chen, M. He, et al., "Lateral Performance of Self-Centering Steel–Timber Hybrid Shear Walls With Slip-Friction Dampers: Experimental Investigation and Numerical Simulation," *Journal of Structural Engineering* 147, no. 1 (2021): 04020291, https://doi.org/10.1061/(ASCE)ST.1943-541X.0002850.

16. S. Jaisee, F. Yue, and Y. H. Ooi, "A State-of-the-Art Review on Passive Friction Dampers and Their Applications," *Engineering Structures* 235 (2021): 112022, https://doi.org/10.1016/j.engstruct.2021.112022.

17. K. Chen, G. Tsampras, and K. Lee, "Structural Connection With Predetermined Discrete Variable Friction Forces," *Resilient Cities and Structures* 2, no. 1 (2023): 1–17, https://www.sciencedirect.com/science/article/pii/S2772741623000066.

18. "Pall dynamics," (2025), accessed: 2025-09-02, https://www.palldynamics.com/FrictionDampers.htm.

19. "Quaketek," (2025), accessed: 2025-09-02, https://quaketek.com/.

20. "Damptech," (2025), accessed: 2025-09-02, https://www.damptech.com/.

10969845, 2026, 6, Downloaded from https://onlinelibrary.wiley.com/doi/10.1002/eqe.70121 by University Of California, Wiley Online Library on [07/11/2026]. See the Terms and Conditions (https://onlinelibrary.wiley.com/terms-and-conditions) on Wiley Online Library for rules of use; OA articles are governed by the applicable Creative Commons License

21. "Oiles corporation," (2025), accessed: 2025-09-02, https://www.oiles.co.jp/en/index.html.

22. "Tectonus," (2025), accessed: 2025-09-02, https://www.tectonus.com/.

23. Z. Zhang, R. B. Fleischman, J. I. Restrepo, et al., "Shake-Table Test Performance of an Inertial Force-Limiting Floor Anchorage System," *Earthquake Engineering & Structural Dynamics* 47, no. 10 (2018): 1987–2011, https://doi.org/10.1002/eqe.3047.

24. C. E. Grigorian, T. S. Yang, and E. P. Popov, "Slotted Bolted Connection Energy Dissipators," *Earthquake Spectra* 9, no. 3 (1993): 491–504, https://doi.org/10.1193/1.1585726.

25. American Society of Civil Engineers, *Minimum Design Loads and Associated Criteria for Buildings and Other Structures (ASCE/SEI 7-22)* (American Society of Civil Engineers, 2022).

26. K. Chen, G. Tsampras, S. Cheruvalath, and M. Thundathil, "Experimental Characterization of Mechanical and Tribological Properties of Composite Materials for Friction-Based Force-Limiting Structural Components," *Composites Part B: Engineering* (2025): 112472, https://doi.org/10.1016/j.compositesb.2025.112472.

27. C. A. Coulomb, *Théorie des Machines Simples (Theory of Simple Machines)* (Bachelier, Paris, 1821).

28. C. J. Black, N. Makris, and I. D. Aiken, "Component Testing, Seismic Evaluation and Characterization of Buckling-Restrained Braces," *Journal of Structural Engineering* 130, no. 6 (2004): 880–894, https://doi.org/10.1061/(ASCE)0733-9445(2004)130:6(880).

29. R. DesRoches, J. McCormick, and M. Delemont, "Cyclic Properties of Superelastic Shape Memory Alloy Wires and Bars," *Journal of Structural Engineering* 130, no. 1 (2004): 38–46, https://doi.org/10.1061/(ASCE)0733-9445(2004)130:1(38).

30. American Institute of Steel Construction, *Steel Construction Manual*, 16th ed. (American Institute of Steel Construction, 2023).

31. G. Tsampras and R. Sause, "Development and Experimental Validation of Deformable Connection for Earthquake-Resistant Building Systems With Reduced Floor Accelerations," (Lehigh University, Technical Report, 2015).

32. M. Latour, V. Piluso, and G. Rizzano, "Free From Damage Beam-to-Column Joints: Testing and Design of DST Connections With Friction Pads," *Engineering Structures* 85 (Feb. 2015): 219–233, https://doi.org/10.1016/j.engstruct.2014.12.019.

33. G. Tsampras and R. Sause, "Full-Scale, Components Test of Inertial Force-Limiting Floor Anchorage Systems for Seismic Resistant Building Structures Using a Friction Device and Carbon Fiber Reinforced Low Damping Rubber Bearings," (2014), accessed: 2025-04-29, https://www.designsafe-ci.org/data/browser/public/nees.public/NEES-2011-1083.groups/Experiment-3.

34. Research Council on Structural Connections, *Specification for Structural Joints Using High-Strength Bolts (RCSC Specification)* (American Institute of Steel Construction, Chicago, IL, 2020).

35. J. Lv, Y. Xiao, and Y. Xue, "Time-Temperature-Dependent Response and Analysis of Preload Relaxation in Bolted Composite Joints," *Journal of Reinforced Plastics and Composites* 37, no. 7 (2018): 460–474, https://doi.org/10.1177/0731684417752082.

36. D. Weerth and C. Ortloff, "Creep Considerations in Reinforced Plastic Laminate Bolted Connections," in *Army Symposium on Solid Mechanics* (1986), 137–154.

37. S. D. Thoppul, R. F. Gibson, and R. A. Ibrahim, "Phenomenological Modeling and Numerical Simulation of Relaxation in Bolted Composite Joints," *Journal of Composite Materials* 42, no. 17 (2008): 1709–1729, https://doi.org/10.1177/0021998308092544.

38. V. Caccese, K. A. Berube, M. Fernandez, J. D. Melo, and J. P. Kabche, "Influence of Stress Relaxation on Clamp-Up Force in Hybrid Composite-to-Metal Bolted Joints," *Composite Structures* 89, no. 2 (2009): 285–293, https://doi.org/10.1016/j.compstruct.2008.07.031.

39. A. Scattina, D. Roncato, G. Belingardi, and G. Martino, "Investigation of Creep Phenomenon on Composite Material for Bolt Connections," *Composite Structures* 134 (2015): 378–383, https://doi.org/10.1016/j.compstruct.2015.08.061.

40. I. H. Mualla and B. Belev, "Performance of Steel Frames With a New Friction Damper Device Under Earthquake Excitation," *Engineering Structures* 24, no. 3 (2002): 365–371, https://doi.org/10.1016/S0141-0296(01)00102-X.

41. S. Ramhormozian, G. Clifton, and G. MacRae, "The Asymmetric Friction Connection With Belleville Springs in the Sliding Hinge Joint," in *Proceedings of 2014 NZSEE Conference* (2014).

42. M. Latour, V. Piluso, and G. Rizzano, "Experimental Analysis on Friction Materials for Supplemental Damping Devices," *Construction and Building Materials* 65 (2014): 159–176, https://doi.org/10.1016/j.conbuildmat.2014.04.092.

43. S. Veismoradi, S. M. M. Yousef-beik, P. Zarnani, and P. Quenneville, "Development and Parametric Study of a New Self-Centering Rotational Friction Damper," *Engineering Structures* 235 (2021): 112097, https://doi.org/10.1016/j.engstruct.2021.112097.

44. A. B. Francavilla, M. Latour, G. Rizzano, F. Nigro, and V. Piluso, "Experimental Assessment of the Hysteretic Response of Resilient Low-Damage Friction Joints With Different Belleville Disk Springs Configurations," *Soil Dynamics and Earthquake Engineering* 180 (2024): 108617, https://doi.org/10.1016/j.soildyn.2024.108617.

45. C.-C. Chou, C.-J. Wu, L.-Y. Huang, et al., "Shaking Table Tests of a Three-Story Re-Centering Steel Braced Frame With Sliding Slab Connected to Energy Dissipation Devices," *Earthquake Engineering & Structural Dynamics* 54, no. 15 (2025): 3746–3767, https://doi.org/10.1002/eqe.70053.

46. G. Tsampras and R. Sause, "Force-Based Design Method for Force-Limiting Deformable Connections in Earthquake-Resistant Buildings," *Journal of Structural Engineering* 148, no. 10 (2022): 04022150, https://doi.org/10.1061/(ASCE)ST.1943-541X.0003456.

47. *Specification for Structural Steel Buildings* (American Institute of Steel Construction, 2022).

48. ANSYS, Inc., *ANSYS Mechanical User's Guide* (ANSYS, Inc., Canonsburg, PA, USA, 2024), release 2024 R1, https://www.ansys.com.

49. "Autodesk," (2025), accessed: 2025-04-10, https://www.autodesk.com/.

50. "Haas," (2025), accessed: 2025-04-10, https://www.haascnc.com/index.html.

51. "Gatke," (2025), accessed: 2025-04-10, https://www.scanpac.com/gatke/.

52. "Onefinity," (2025), accessed: 2025-04-18, https://www.onefinitycnc.com.

53. "Correlated solutions," (2025), accessed: 2025-04-10, https://www.correlatedsolutions.com/.

54. R. Cox, *Engineered Tribological Composites* (SAE International, Warrendale, PA, Nov. 2011).

55. A. Córdova, C.-C. Chou, C.-J. Wu, G. Tsampras, C.-M. Uang, and S.-H. Chao, "Modeling and Response of a Three-Story Steel Building With Sliding Slabs in Earthquake Motions," *Earthquake Engineering & Structural Dynamics* 54, no. 3 (2025): 1101–1121, https://doi.org/10.1002/eqe.4300.

56. P. J. Blau, *Friction Science and Technology: From Concepts to Applications* (CRC press, 2008).

57. C.-M. Lin, Y.-W. Chang, C.-C. Chou, et al., "Reconnaissance of the 2022 Guanshan and Chihshang Earthquakes in Eastern Taiwan," *Earthquake Spectra* 40, no. 1 (2024): 531–565, https://doi.org/10.1177/87552930231209102.

10969845, 2026, 6, Downloaded from https://onlinelibrary.wiley.com/doi/10.1002/eqe.70121 by University Of California, Wiley Online Library on [07/11/2026]. See the Terms and Conditions (https://onlinelibrary.wiley.com/terms-and-conditions) on Wiley Online Library for rules of use; OA articles are governed by the applicable Creative Commons License